Earth-Science Reviews 211 (2020) 103210

Contents lists available at ScienceDirect

Earth-Science Reviews

journal homepage: www.elsevier.com/locate/earscirev

Comparability of heavy mineral data – The first interlaboratory round robin test

István Dunkl[a,*], Hilmar von Eynatten[a], Sergio Andò[b], Keno Lünsdorf[a], Andrew Morton[c], Bruce Alexander[d], László Aradi[e], Carita Augustsson[f], Heinrich Bahlburg[g], Marta Barbarano[h], Aukje Benedictus[i], Jasper Berndt[j], Irene Bitz[k], Flora Boekhout[g], Tim Breitfeld[l], João Cascalho[m], Pedro J.M. Costa[n], Ogechi Ekwenye[o], Kristóf Fehér[p], Valentina Flores-Aqueveque[q], Philipp Führing[a], Paulo Giannini[r], Walter Goetz[s], Carlos Guedes[t], György Gyurica[u], Juliane Hennig-Breitfeld[l,v], Julian Hülscher[w], Mahdi Jafarzadeh[x], Robert Jagodziński[y], Sándor Józsa[p], Péter Kelemen[p], Nynke Keulen[z], Marijan Kovacic[aa], Christof Liebermann[l], Mara Limonta[b], Borna Lužar-Oberiter[ab], Frane Markovic[aa], Frank Melcher[ac], Dóra Georgina Miklós[p], Ogechukwu Moghalu[o], Ian Mounteney[ad], Daniel Nascimento[ae], Tea Novaković[ab], Gabriella Obbágy[af], Mathias Oehlke[s], Jenny Omma[i], Peter Onuk[ac], Sandra Passchier[ag], Katharina Pfaff[ah], Luisa Pinto Lincoñir[ai], Matthew Power[aj], Ivan Razum[ak], Alberto Resentini[b], Tamás Sági[p], Dorota Salata[al], Rute Salgueiro[am], Jan Schönig[a], Maria Sitnikova[an], Beata Sternal[y], György Szakmány[p], Monika Szokaluk[ao], Edit Thamó-Bozsó[ap], Ágoston Tóth[p], Jonathan Tremblay[aq], Jasper Verhaegen[ar], Tania Villaseñor[ai], Michael Wagreich[as], Anna Wolf[a], Kohki Yoshida[at]

[a] Department of Sedimentology and Environmental Geology, Geoscience Center, University of Göttingen, Goldschmidtstr. 3, D-37077 Göttingen, Germany
[b] Department of Earth and Environmental Sciences, University of Milano Bicocca, Piazza della Scienza 4, I-20126 Milano, Italy
[c] HM Research Associates, Giddanmu, Musselwick Road, St Ishmaels, Pembrokeshire SA62 3TJ, UK
[d] School of Science, University of Greenwich, Central Avenue, Chatham Maritime, Kent ME4 4TB, UK
[e] Lithosphere Fluid Research Laboratory, Eötvös Loránd University, Pázmány P. sétány 1/C, H-1117 Budapest, Hungary
[f] Institutt for Energiressurser, N-4036 Stavanger, Norway
[g] Institut für Geologie und Paläontologie, Westfälische Wilhelms-Universität, Corrensstrasse 24, D-48149 Münster, Germany
[h] Chemostrat Ltd 1, Ravenscroft Court, Buttington Enterprise Park, Welshpool SY21 8SL, UK

* Corresponding author.
E-mail addresses: istvan.dunkl@geo.uni-goettingen.de (I. Dunkl), hilmar.von.eynatten@geo.uni-goettingen.de (H. von Eynatten), sergio.ando@unimib.it (S. Andò), kluensd@gwdg.de (K. Lünsdorf), heavyminerals@hotmail.co.uk (A. Morton), B.Alexander@greenwich.ac.uk (B. Alexander), aradi.laszloelod@gmail.com (L. Aradi), carita.augustsson@uis.no (C. Augustsson), bahlbur@uni-muenster.de (H. Bahlburg), martabarbarano@chemostrat.com (M. Barbarano), aukje.benedictus@rocktype.com (A. Benedictus), jberndt@uni-muenster.de (J. Berndt), Irene.Bitz@lbeg.niedersachsen.de (I. Bitz), boekhout@uni-muenster.de (F. Boekhout), t.breitfeld@es.rhul.ac.uk (T. Breitfeld), jpcascalho@fc.ul.pt (J. Cascalho), ppcosta@dct.uc.pt (P.J.M. Costa), ogechi.ekwenye@unn.edu.ng (O. Ekwenye), lorcs@hotmail.hu (K. Fehér), v.flores.a@gmail.com (V. Flores-Aqueveque), philipp.fuehring@stud.uni-goettingen.de (P. Führing), pcgianni@usp.br (P. Giannini), goetz@mps.mpg.de (W. Goetz), ccfguedes@gmail.com (C. Guedes), gyuricza.gyorgy@mbfsz.gov.hu (G. Gyurica), j.hennig@es.rhul.ac.uk (J. Hennig-Breitfeld), julian.huelscher@fu-berlin.de (J. Hülscher), m_jafarzadeh@shahroodut.ac.ir (M. Jafarzadeh), jagodus@amu.edu.pl (R. Jagodziński), sandor-jozsa@caesar.elte.hu (S. Józsa), kelemenpeter1991@gmail.com (P. Kelemen), ntk@geus.dk (N. Keulen), marijan.kovacic@gfz.hr (M. Kovacic), chris.liebermann@gmail.com (C. Liebermann), mara.limonta@unimib.it (M. Limonta), bluzar@geol.pmf.hr (B. Lužar-Oberiter), frane.markovic@geol.pmf.hr (F. Markovic), Frank.Melcher@unileoben.ac.at (F. Melcher), miklosdoragina94@gmail.com (D.G. Miklós), ogechukwu.moghalu@unn.edu.ng (O. Moghalu), iaian1@bgs.ac.uk (I. Mounteney), daniel.rodrigues@ufc.br (D. Nascimento), teanovakovic@gmail.com (T. Novaković), obbagy.gabriella@atomki.mta.hu (G. Obbágy), oehlke@gmx.de (M. Oehlke), jenny.omma@rocktype.com (J. Omma), Peter.Onuk@unileoben.ac.at (P. Onuk), passchiers@mail.montclair.edu (S. Passchier), kpfaff@mines.edu (K. Pfaff), lpinto@ing.uchile.cl (L.P. Lincoñir), matt@powerotero.com (M. Power), irazum@hpm.hr (I. Razum), alberto.resentini@unimib.it (A. Resentini), sagi.tamas@ttk.elte.hu (T. Sági), dorota.salata@uj.edu.pl (D. Salata), rute.salgueiro@lneg.pt (R. Salgueiro), jan.schoenig@uni-goettingen.de (J. Schönig), MariaAlexandrovna.Sitnikova@bgr.de (M. Sitnikova), sternal@amu.edu.pl (B. Sternal), szakmany@caesar.elte.hu (G. Szakmány), monika.szokaluk@amu.edu.pl (M. Szokaluk), bozso.edit@mbfsz.gov.hu (E. Thamó-Bozsó), toth.agoston01@gmail.com (Á. Tóth), jtremblay@iosgeo.com (J. Tremblay), jasper.verhaegen@kuleuven.be (J. Verhaegen), tania.villasenor.j@gmail.com (T. Villaseñor), michael.wagreich@univie.ac.at (M. Wagreich), anna.fe@gmx.de (A. Wolf), kxyoshid@shinshu-u.ac.jp (K. Yoshida).

https://doi.org/10.1016/j.earscirev.2020.103210

Available online 16 June 2020

[i] Rocktype Ltd, 87 Divinity Road, Oxford OX4 1LN, UK
[j] Institut für Mineralogie, Westfälische Wilhelms-Universität, Corrensstrasse 24, D-48149 Münster, Germany
[k] Landesamt für Bergbau, Energie und Geologie Geozentrum, Hannover, Germany
[l] Queens Building SE Asia Research Group Earth Sciences Department, Royal Holloway University of London, Egham Hill EGHAM, Surrey TW20 0EX, UK
[m] Instituto D. Luiz and Departamento de Geologia, Universidade de Lisboa, Edifício C6, Campo Grande, 1749-016 Lisboa, Portugal
[n] Departamento de Ciências da Terra, Universidade de Coimbra, Coimbra, Portugal
[o] Department of Geology, University of Nigeria, Nsukka 410001, Enugu State, Nigeria
[p] Department of Petrology & Geochemistry, Eötvös University, Pázmány P. sétány 1/C, H-1117 Budapest, Hungary
[q] ARQMAR Centre for Maritime Archaeology Research of the Southeastern Pacific, Casilla 21, 2340000, Valparaiso, Chile
[r] Institute of Geosciences, University of São Paulo Rua do Lago, 562, Cidade Universitária, Butantã 05508-080, São Paulo, Brazil
[s] Max-Planck-Institut für Sonnensystemforschung, Justus-von-Liebig-Weg, 3, D - 37077 Göttingen, Germany
[t] Geology department, Universidade Federal do Paraná, Av. Cel. Francisco H. dos Santos, 210 - Jardim das Américas, – Curitiba PR 81531-980, Brazil
[u] Department of Applied and Environmental Geology, Mining and Geological Survey of Hungary, Stefánia út 14 H-1143, Budapest, Hungary
[v] Department of Earth Sciences Egham Hill, Royal Holloway University of London, Egham TW20 0EX, UK
[w] Institut für geologische Wissenschaften Tektonik und Sedimentäre Systeme, Freie Universität Berlin, Malteserstr. 74-100, D-12249 Berlin, Germany
[x] Faculty of Earth Sciences, Shahrood University of Technology, Hafte-Tir square, Shahrood, Iran
[y] Geohazards Lab, Institute of Geology, Adam Mickiewicz University in Poznań, Bogumiła Krygowskiego 12, PL-61-680 Poznań, Poland
[z] Department of Petrology and Economic Geology, Geological Survey of Denmark and Greenland, Øster Voldgade 10, DK-1350, Copenhagen K, Denmark
[aa] Department of Geology, Institute of Mineralogy and Petrology, University of Zagreb, Horvatovac 95, HR-10000 Zagreb, Croatia
[ab] Department of Geology, Faculty of Science, University of Zagreb Geološko-paleontološki zavod, Prirodoslovno-matematički fakultet, Horvatovac 102a, HR-10000 Zagreb, Croatia
[ac] Chair of Geology and Economic Geology, Montanuniversität Leoben, Peter-Tunner-Straße 5, A-8700 Leoben, Austria
[ad] British Geological Survey, Knicker, Hill Keyworth, NG12 5GG Nottingham, UK
[ae] Departamento de Geologia, Universidade Federal do Ceará, Campus do PICI, Bloco 912 60440-554, Fortaleza (CE), Brazil
[af] Institute for Nuclear Research, Hungarian Academy of Sciences, Bem square 18/c, H-4026 Debrecen, Hungary
[ag] Department of Earth and Environmental Studies, Montclair State University, CELS 220, 1 Normal Ave, Montclair, NJ 07043, USA
[ah] Colorado School of Mines, 1516 Illinois Street, Golden, CO 80401, USA
[ai] Departmento de Geologia, FCFM, Universidad de Chile, Plaza Ercilla 803, Casilla 13518, Correo 21, Santiago, Chile
[aj] Oil, Gas & Chemicals Services, SGS Canada Inc., 3260 Production Way, Burnaby, BC V5A 4W4, Canada
[ak] Croatian Natural History Museum, Demetrova 1, HR-10000 Zagreb, Croatia
[al] Faculty of Geography and Geology, Institute of Geological Sciences, Jagiellonian University, Gronostajowa 3a, PL-30-387 Krakow, Poland
[am] LNEG-Laboratório Nacional de Energia e Geologia, Estrada da Portela, Bairro do Zambujal, Apartado 7586- Alfragide, 2610-999 Amadora, Portugal
[an] BGR B2.1 Geophysikalische Erkundung - Technische Mineralogie, Stilleweg 2, D-30655 Hannover, Germany
[ao] Department of Mineralogy and Petrology, Institute of Geology, Adam Mickiewicz University in Poznan, str. Bogumila Krygowskiego 12, PL-61-680 Poznan, Poland
[ap] Department of Geological Basic Research, Mining and Geological Survey of Hungary, Stefánia út 14, H-1143 Budapest, Hungary
[aq] IOS Services Geoscientifiques Inc, 1319 St-Paul Boulevard, Saguenay, Québec G7J 3Y2, Canada
[ar] Department of Earth and Environmental Sciences, KU Leuven, Celestijnenlaan 200E, B-3001 Heverlee, Belgium
[as] Department of Geodynamics and Sedimentology, Center for Earth Sciences, University of Vienna, Althanstrasse 14, A-1090 Vienna, Austria
[at] Department of Geology, Faculty of Science Shinshu University, Asahi 3-1-1, Matsumoto 390-8621, Nagano Prefecture, Japan

ARTICLE INFO

Keywords:
Heavy mineral analysis
Provenance
SEM-EDX
Raman spectroscopy
Interlaboratory comparison

ABSTRACT

Heavy minerals are typically rare but important components of siliciclastic sediments and rocks. Their abundance, proportions, and variability carry valuable information on source rocks, climatic, environmental and transport conditions between source to sink, and diagenetic processes. They are important for practical purposes such as prospecting for mineral resources or the correlation and interpretation of geologic reservoirs. Despite the extensive use of heavy mineral analysis in sedimentary petrography and quite diverse methods for quantifying heavy mineral assemblages, there has never been a systematic comparison of results obtained by different methods and/or operators. This study provides the first interlaboratory test of heavy mineral analysis.

Two synthetic heavy mineral samples were prepared with considerably contrasting compositions intended to resemble natural samples. The contributors were requested to provide (i) metadata describing methods, measurement conditions and experience of the operators and (ii) results tables with mineral species and grain counts. One hundred thirty analyses of the two samples were performed by 67 contributors, encompassing both classical microscopic analyses and data obtained by emerging automated techniques based on electron-beam chemical analysis or Raman spectroscopy.

Because relatively low numbers of mineral counts (N) are typical for optical analyses while automated techniques allow for high N, the results vary considerably with respect to the Poisson uncertainty of the counting statistics. Therefore, standard methods used in evaluation of round robin tests are not feasible. In our case the 'true' compositions of the test samples are not known. Three methods have been applied to determine possible reference values: (i) the initially measured weight percentages, (ii) calculation of grain percentages using estimates of grain volumes and densities, and (iii) the best-match average calculated from the most reliable analyses following multiple, pragmatic and robust criteria. The range of these three values is taken as best approximation of the 'true' composition.

The reported grain percentages were evaluated according to (i) their overall scatter relative to the most likely composition, (ii) the number of identified components that were part of the test samples, (iii) the total amount of mistakenly identified mineral grains that were actually not added to the samples, and (iv) the number of major components, which match the reference values with 95% confidence.

Results indicate that the overall comparability of the analyses is reasonable. However, there are several issues with respect to methods and/or operators. Optical methods yield the poorest results with respect to the scatter of the data. This, however, is not considered inherent to the method as demonstrated by a significant number of optical analyses fulfilling the criteria for the best-match average. Training of the operators is thus considered paramount for optical analyses. Electron-beam methods yield satisfactory results, but problems in the identification of polymorphs and the discrimination of chain silicates are evident. Labs refining their electron-beam results by optical analysis practically tackle this issue. Raman methods yield the best results as indicated by the

highest number of major components correctly quantified with 95% confidence and the fact that all laboratories and operators fulfil the criteria for the best-match average. However, a number of problems must be solved before the full potential of the automated high-throughput techniques in heavy mineral analysis can be achieved.

1. Introduction[1]

Heavy mineral (HM) analysis is a fundamental technique in sedimentary petrography and provenance analysis. It principally serves to quantify the concentration and proportions of accessory minerals with density exceeding 2.85–2.90 g/cm^3 and is typically applied to sand-sized sediments and sedimentary rocks. The occurrence and frequency of these minerals are considered indicative for a variety of geologic conditions and sedimentary processes, including type and characteristics of the source rocks in the drainage system, chemical alteration at the source and in transit, hydrodynamic fractionation during sediment transport and final deposition, and diagenetic overprint in the sedimentary basin.

Separation, microscopic detection, and frequency estimation of heavy minerals have been applied since the 19th century, mainly for reasons of palaeogeographical reconstruction and mineral prospecting (e.g., De Filippi, 1839; Meunier, 1877; Thürach, 1884; Dick, 1887; Artini, 1891; Retgers, 1895). Since that time, heavy mineral analysis developed into an integral part of sedimentary petrography as witnessed by classical textbooks of the first half of the 20th century, which dedicated large parts to the description of heavy minerals (e.g., Milner, 1929; Boswell, 1933). Rubey (1933) demonstrated that the factors controlling heavy mineral distribution in natural samples are numerous and complex, and emphasized the role of hydraulic size-density sorting. Thus, grain-size control is crucial for the interpretation of heavy mineral data, which typically come from minerals with a considerable range in density. From about the 1960s to the 1980s heavy mineral analysis was out-of-favour, likely related to the advent of new concepts in sedimentary geology such as detailed facies models (Walker, 1979), plate tectonics and sandstone framework composition (e.g., Dickinson and Suczek, 1979) and seismic stratigraphy and sequence stratigraphy (Vail et al., 1977). The revival of heavy mineral analysis started in the 1980s partly due to the advent of techniques such as single-grain mineral chemistry (e.g., Mange-Rajetzky, 1981; Morton, 1985) and geochronology (e.g., Dodson et al., 1988). Since then a wide range of analytical techniques is routinely used to study geochemical and isotopic composition of individual sand-sized grains (e.g., von Eynatten and Dunkl, 2012). Besides technical progress, heavy mineral analysis has also become important for research in fields like the interaction of tectonics and sedimentation (especially in young mountain belts where precise chronostratigraphy constrains rates of orogenic evolution), landscape evolution, and more generally, the links between source and sink in sediment routing systems (e.g., Allen, 2017). Nowadays, heavy mineral analysis is used in various academic branches of geology, mineralogy, geochemistry, geomorphology and geoarchaeology as well as interdisciplinary research topics such as forensic investigations and exploration for various natural resources (e.g., Mange and Wright, 2007; Garzanti and Andò, 2019).

The analysis of heavy mineral assemblages is traditionally performed optically using the polarizing microscope (Mange and Maurer, 1992), which still appears to be the most frequently used technique. Other rarely used techniques include geochemical analysis (e.g., Mounteney et al., 2018) and X-ray diffraction phase analysis (e.g., Webster et al., 2003) of the bulk heavy mineral fraction. The last decade has brought up new developments in the analysis of heavy mineral assemblages based on (i) electron beam methods (mostly combinations of scanning electron microscopy (SEM) and energy-dispersive X-ray spectroscopy (EDX); e.g., Bernstein et al., 2008; Sylvester, 2012; Zhang et al., 2015) and (ii) Raman spectroscopic methods (e.g., Andò et al., 2009; Andò and Garzanti, 2014; Lünsdorf et al., 2019).

Despite the extensive use of heavy mineral data for a wide range of geoscientific and related problems, there is neither a generally accepted approach to the generation of data nor a widely accepted set of standardized samples to assess laboratory accuracy and precision. This is in strong contrast to many branches of analytical, technological and health research, where strictly organized analysis rounds in numerous laboratories on test materials of known or unknown properties are common. The goals of such tests include (i) determination of the 'true' values in search of future reference materials, (ii) examination and self-calibration of an individual laboratory, (iii) certification or accreditation of laboratories, and (iv) getting an overview on the comparability and/or reproducibility of the results of a given analytical method or a specific procedure. Such tests are organized under various conditions and are called Round Robin Test (RRT), Inter Laboratory Comparison/Comparability tests (ILC) or Proficiency Testing (PT). National and international standards offer constraints for the planning, realization and evaluation of the results like ASTM E691: 2013, ASTM E1301-95, 2003, ISO 21748, 2017 and ISO/IEC 17043, 2010. Nowadays state-of-the-art analytical facilities actually need regular control using reference materials and participation in inter-laboratory tests. In geosciences, RRTs are commonly used for diverse analytical methods, for instance, fission track thermochronology (Miller et al., 1990; Ketcham et al., 2015), U−Pb geochronology (Košler et al., 2013), coal petrography (Finkelman et al., 1984), vitrinite reflectance (Hackley et al., 2015) and isotope ratios (Gonfiantini et al., 2003). However, a test of the comparability, precision, or reproducibility of mineral identification in sand-sized samples involving a large number of laboratories and different analytical techniques has not yet been carried out.

This study provides the first interlaboratory comparison of heavy mineral analysis and quantification. Two different samples of synthetic mixtures of several mineral species were prepared. A call for participation was distributed via e-mail lists and a webpage in December 2017 and the samples were shipped upon request in spring 2018. The contributors were asked to process the samples according to their usual laboratory routines. Altogether 67 contributors provided 130 analyses of the two samples (65 individual result reports with two samples each). We received 92 optical analyses by microscopic methods, 24 chemical analyses by electron beam methods and 14 mineralogical-crystallographical analyses, including 12 by Raman spectroscopic methods and 2 by X-ray diffraction. All contributors are co-authors of this paper.

2. Techniques and problems associated with heavy mineral quantification

This section aims at giving a brief review of some of the intrinsic problems associated with heavy mineral quantification, from sampling in the field or core repository via the various steps of mineral separation and preparation to the final mineral determination and quantification procedures. It is intended to foster understanding of the complexity of separating and quantifying a (typically) small fraction of size and density fractionated grains from a sediment sample. It is not intended to provide a full review of techniques and applications in heavy mineral analysis. For the latter the reader is referred to other studies and textbooks, among them *Heavy Minerals in Colour* (Mange and Maurer, 1992), the voluminous compilation in *Heavy Minerals in Use* (Mange and Wright, 2007) and some review papers on general and specific

[1] For the explanation of abbreviations and definitions used in this work, see, please Appendix A.

aspects in heavy mineral research (e.g., Andò et al., 2012; Morton, 2012; von Eynatten and Dunkl, 2012; Garzanti and Andò, 2019).

The problems may be subdivided into (i) sampling, (ii) grain-size range selected for analysis, (iii) laboratory separation, splitting, and preparation procedures, (iv) counting techniques, and, partly related (v) the method used to identify the individual mineral species. All of these issues contribute to the overall variability and significance of the results (e.g., Morton, 2012; Garzanti and Andò, 2019).

2.1. Sampling

Taking a representative sample in the field or core repository introduces the first level of uncertainty. As there is mostly no indication of 'representativeness', we have to accept that sampling forms a principal source of error. This fundamental problem is not specific to heavy mineral analysis. It is inherent to many approaches in geosciences, where small samples (typically few hundred grams up to few kilograms) are taken in order to represent comparatively huge volumes of sediment or rock. Minimizing this error for heavy mineral analysis calls for a strict sampling plan intended to maximise consistency and comparability among samples, which should include (i) avoiding selection based on particular properties (e.g., colour, components, grain size, sorting), (ii) seeking for samples with grain size in the fine to medium sand range (i.e. 125 to max. 500 μm), (iii) sampling similar grain size for sample sets that are going to be compared (e.g., Mange and Maurer, 1992; Garzanti and Andò, 2019).

2.2. Grain-size range for analysis

The frequency and proportions of heavy minerals depend on the grain size considered (e.g., Rubey, 1933; Boenigk, 1983). Besides initial sampling of an appropriate grain size range (see above), the grain size range used for analysis is relevant. This is largely due to hydrodynamic effects leading to enrichment of certain mineral species in the coarse- or fine-grained tails of the distribution. It has been summarized and demonstrated by Garzanti et al. (2008) using various environments and a multiple grain-size 'window' strategy (i.e. analysis over a wide grain size range at small 0.25–0.5 phi steps). Applying corrections based on estimated mineral densities can eliminate the hydrodynamic effects contributing to natural heavy mineral assemblages (Garzanti et al., 2009). Using multiple grain size windows or a single wide window (e.g., 15–500 μm) thus reduces the analytical bias. However, grain-size relations in heavy mineral analyses are not only controlled by hydrodynamics based on density. Other controls on heavy mineral composition, which cannot be easily restored based on simple physical laws, include textural features affecting hydrodynamic behaviour of the grains (i.e. shape and surface roughness), inherited grain-size distributions from the source rocks, as well as various effects of grain alteration during weathering and diagenesis, and precipitation of authigenic phases during diagenesis (e.g., TiO_2 minerals). Because of these uncertainties, especially in the case of ancient sedimentary rocks, and for practical reasons (mounting and microscopic identification is deemed easier for narrow sand-sized fractions by several users), many heavy mineral studies still use narrow grain-size fractions such as 63–125 μm or 63–250 μm (Morton, 2012).

2.3. Laboratory procedures

After liberation of the grains by crushing and/or dissolution of the cement (for sedimentary rocks) and sieving, the heavy minerals are separated from the selected grain size fraction of the sample using heavy liquids (mostly the toxic bromoform but nowadays mainly sodium or lithium polytungstate) and gravity settling or centrifuge. The heavy mineral fraction typically needs to be split to get a suitable amount of minerals for mounting on microscopic slides. Just sprinkling some part from a vial onto the slide induces significant sorting due to size, density and shape. Carelessness at this step must be considered as a major source of error in HM preparation (Mange and Maurer, 1992; Andò, 2020). Besides often-criticized techniques such as taking a microsample from somewhere in the middle of the vial, two main approaches have been suggested for splitting small volumes of granular material: (i) especially designed micro splitters or (ii) coning and quartering (Mange and Maurer, 1992). After splitting the sample is mounted on glass slides using various embedding media, which may help with optical identification depending on their refractive index. If no further analyses are planned, slides are typically covered with glass. In the case of electron beam and Raman spectroscopical methods, the grain mounts are uncovered and polished after embedding e.g., in epoxy resin.

2.4. Counting technique

Because the mineral grains are irregularly distributed on the slides, point-counting devices (e.g., Chayes, 1949) were initially considered inappropriate for heavy mineral counting. Instead, different techniques have been developed, starting with Fleet (1926) who suggested counting all minerals on the slide to provide relative abundances as grain percentages (called the Fleet method). More pragmatic approaches suggested to count only a portion of the mineral grains on the slide include line counting, i.e. the slide is moved mechanically along linear traverses and grains intersecting with the crosshair of the microscope are counted, and ribbon counting, i.e. the slide is moved similarly but all grains within randomly selected bands (ribbons) are counted (Mange and Maurer, 1992). While the former technique is obviously sensitive to grain size, the latter is thought to be insensitive to grain size. In the case of wide grain size windows and/or if the counting technique aims at areal percentages, point-counting is the method of choice (Garzanti and Andò, 2019).

2.5. Method used for mineral identification

The traditional and still most frequently used technique for heavy mineral identification is based on optical properties using the polarizing microscope (e.g., Mange and Maurer, 1992). It has the potential to assess the full range of optical (colour, pleochroism, refractive index, birefringence, etc.) and morphological features (habit, cleavage and especially corrosion, e.g., Andò et al., 2012), which may be very useful for identification and discrimination. However, optical identification by polarizing microscope has some drawbacks, mainly (i) problems in identification caused by, for instance, overlapping optical properties, different orientations of optically anisotropic grains and/or the difficulties from the fuzzy properties in the case of monomineralic but polycrystalline grains, and (ii) opaque minerals that cannot be distinguished in transmitted light (Morton, 2012). The former can be partly overcome by well-trained operators (reducing the operator bias), and the latter by using polished mineral mounts and reflected light microscopy.

SEM-EDX and Raman spectroscopic methods potentially allow for (i) counting a large number of grains per sample, high sample throughput and thus higher spatial and temporal resolution in heavy mineral analysis, (ii) better precision and reproducibility of HM identification, (iii) including opaque phases in heavy mineral analysis, (iv) providing additional compositional information on individual phases, and (v) efficient screening for specific phases that can be used for other measurements such as detrital geochronology on the same slides (e.g., Zhang et al., 2015; Vermeesch et al., 2017; Lünsdorf et al., 2019). Moreover, these techniques allow for analysis of finer fractions (i.e. medium to coarse silt), which opens the door towards including fine-grained sediment and pelitic rocks in provenance studies (e.g., Andò et al., 2011; Caracciolo et al., 2019; Paleari et al., 2019). Specific drawbacks of these methods include the inability to discriminate polymorphs (e.g., rutile-anatase-brookite, kyanite-sillimanite-andalusite) in the case of SEM-EDX techniques. While Raman techniques

enable polymorph identification, current problems are related to, for instance, complex spectra caused by luminescence/fluorescence effects and members of solid solution series, which are not properly covered by the current data bases, as well as composite spectra of multiple phases, in particular for inclusion-rich grains. Furthermore, these techniques do not supply information on grain colour or habit (e.g., surface corrosion), which may be important for interpreting the ensuing data.

3. Concept, preparation and distribution of test samples

3.1. Concept for composing the HMR test samples

Two main options are available for composing the samples for such an interlaboratory test: (i) carefully selected and homogenized natural HM samples that contain a wide range of mineral species or (ii) artificial sand-sized mineral mixtures including commonly occurring heavy minerals. The first option has the advantage that the contributors would observe natural grains resulting from the typical process chain of weathering, erosion, transport, deposition and, maybe, diagenetic processes implying that their morphological features are 'typical', so that their appearance is familiar to the contributors. On the other hand, natural samples contain lithic fragments (i.e. grains composed of more than one mineral), coated grains, minerals altered to varying degrees, and/or opaque phases. Because a widely used and accepted analytical procedure is lacking, the presence of such grains increases subjectivity and introduces additional uncertainties in comparing the results. Therefore we decided to perform the interlaboratory test with synthetic heavy mineral samples. In this way the vast majority of the grains is monomineralic, lithic fragments are absent, and the artificial target composition can be controlled by mixing well characterized mineral samples.

The HMR test samples were mixed from six to seven major and several minor components (see Appendix A for definitions). The major components were around 10 wt% or higher in concentration and their abundances should allow for reliable quantification of the respective mineral or mineral group. In the case of the minor components, mostly between 1 and 4 wt%, the main goal of the test was their recognition only. When only a few hundred grains are counted (such as with the optical method) there are corresponding high counting errors, thus the quantification of the minor components is not considered reliable.

Two test samples were created; HMR-1 aimed to mimic the composition of sediment derived from an orogenic source mainly composed of metapelitic and metabasic rocks. It was characterized by the ultrastable minerals zircon (rounded), tourmaline, and rutile along with garnet, Al-silicates, staurolite, epidote and as minor components amphibole, apatite, anatase, brookite and traces from ultramafic rocks, olivine and chromian spinel (Table 1). HMR-2 aimed to mimic the composition of sediment derived from a catchment dominated by igneous rocks that also contains some ore bodies. This sample was composed of zircon (both euhedral and rounded), apatite, titanite, pyroxene, amphibole, epidote group minerals and as minor components of rutile, garnet, corundum, fluorite, baryte, topaz, cassiterite and scheelite (see details below).

Heavy mineral analyses were performed on different grain size fractions in different laboratories, as outlined in Section 2. The selection of grain size has profound control on heavy mineral composition and some counting techniques are also biased by grain size. In order to minimize these effects, we decided to use a narrow grain size fraction for the test samples, i.e. 63–125 μm. Depending on mineral shape, long axes might be considerably longer than 125 μm.

3.2. Mineral samples used for the synthetic mixtures and the preparation procedure

We tested 61 mineral samples for their appearance, homogeneity and purity. 40 of these were selected as mineral samples for the final HMR samples (Table 2). For zircon, tourmaline, rutile, apatite, garnet, titanite, pyroxene, amphibole and the epidote group different varieties were used, in order to simulate some of the variability typically occurring in natural samples. For instance, the five amphibole varieties include typical green hornblende (DM-69), pale coloured tremolite-rich amphibole (A993), colourless tremolite (DM-73), brown 'oxy-hornblende' (DM-99) and blue amphibole (DM-78). Differently coloured varieties were also used for garnet, tourmaline, titanite, pyroxene, epidote group minerals, and cassiterite. In the case of zircon, tourmaline, rutile and apatite, both rounded and euhedral grains were included (Fig. 1, a-f, and Table 2). Other euhedral grains included orthopyroxene (typical in volcanic rocks) and baryte (may occur as an authigenic phase in sedimentary rocks). The shape of the other minerals is less critical because most of them (e.g., garnet, Al-silicates, staurolite, amphibole) are typically larger in the source rocks than the very fine sand fraction (63–125 μm) used here. These minerals thus occur as more-or-less rounded anhedral grains or fragments with shapes that are generally determined by the cleavage planes (Fig. 1, g and h).

The starting materials for the mineral samples were either pure monomineralic heavy mineral fractions from a beach placer (DM-126, Table 2) or high purity monocrystals or polycrystals of several mm to cm in size. The latter were crushed and air-abraded in order to (i) further disintegrate shards that were only partly split and (ii) cause some rounding along tips and edges. Air abrasion forms an essential step in the preparation of the synthetic heavy minerals as natural grains lose their sharp corners after relatively short transport and thin shards that are typical of coaxially crushed materials disintegrate quickly. In the case of the big crystal starting materials, the procedure was the following: (1) crushing, (2) sieving to 63–160 μm, i.e. to a grain size with a slightly coarser upper limit compared to the target fraction, (3) if necessary, physical and chemical purification by magnetic separation, heavy liquid separation and nitric acid treatment, (4) air abrasion, (5) cleaning in alcohol, and (6) sieving into the target grain size fraction of 63–125 μm. Air abrasion was performed by a slightly modified device

Table 1
Composition of the synthetic heavy mineral samples.

Component	HMR-1		HMR-2	
	wt%	Grain%	wt%	Grain%
Zircon	***10.2***	***6.3***	***11.1***	***6.9***
Tourmaline	***13.0***	***12.2***		
Rutile	***10.2***	***9.1***	4.0	3.7
Anatase	2.0	1.3		
Brookite	1.3	0.7		
TiO_2 total	***13.5***	***11.1***	4.0	3.7
Apatite	3.7	6.3	***8.9***	***11.4***
Garnet	***10.0***	***10.8***	3.0	1.7
Kyanite	7.9	6.1		
Sillimanite	3.4	2.3		
Andalusite	2.0	2.3		
Al_2SiO_5 total	***13.3***	***10.7***		
Staurolite	***9.9***	***11.2***		
Titanite			***9.9***	***8.4***
Olivine	2.0	2.3		
Cr-spinel	3.0	3.5		
Pyroxene			***17.2***	***18.7***
Amphibole	6.1	7.9	***18.3***	***23.9***
Epidote group	***15.0***	***17.7***	***15.0***	***15.3***
Corundum			2.0	2.5
Fluorite			2.0	1.7
Baryte			2.0	0.7
Topaz			2.0	2.8
Cassiterite			2.0	1.0
Scheelite			2.0	1.2

The calculation of grain percentages from weight percentages is documented in the Electronic Appendix Table EA 1. Bold-Italics numbers are the major components aimed for quantification.

Table 2
Mineral samples used for the HMR synthetic heavy mineral samples and their preparation steps.

Component	Mineral sample	Specification	euhedral	acessory	rock forming	fissure filling	monocrystal or polycrystal crushed and abraded	Host lithology	Locality	Crushing	Sieving 63-160	Magn. sep.	Heavy liquid	Chemical treatment	Air abr.	Washing	Sieving 63-125	Mass [g]	Pureness [%]	Other mineral phases
Zircon	Zm-eu	pinkish-yellowish	e	a				granitoids	Lhasa terrane, Tibet	x	x	x	x	HNO_3				0.32	>99.5	
	DM-126	naturally rounded		a				beach placer	Australia									>10	>99.5	
Tourmaline	DM-114	dark, bluish>brownish					m	pegmatite	Minas Gerais, Brasil	x	x				x	x	x	0.58	>99.5	
	3-246	brown	e	a				contact rock	Manikyangsa, Bhutan	x	x	x	x			x		>10	>99.5	with Qtz inclusions
Rutile	DM-45	dark					m	chlorite schist	Clermont Mills, Harford Co., Maryland, USA	x	x				x	x	x	0.50	>99.9	
	SZ2	brown	e	a				granulite	Ivrea body, Southern Alps	x	x	x	x			x		0.50	>99.5	
Anatase	DM-56	blue + yellow				f	m		Baluchistan, Khuyan village, Pakistan	x	x				x	x		0.30	~99	
Brookite	TX-7	amber-brown				f	m		Baluchistan, Kharan, Pakistan	x	x	x				x		0.61	~85	Rt, Qtz, Apa
Apatite	APM-17-9	colourless	e	a				granitoids	Sierras Pampeanas, Argentina	x	x	x	x			x	x	0.82	~80	Zrn
	AS-16	colourless					m	alkali intrusion	Ilmichil, Morocco	x	x				x	x	x	0.77	~98	lithic fr.
Garnet	DX-80	almandine			r			micaschist	Schneeberger zone, Ötztal, E. Alps	x	x				x	x	x	2.20	>99.9	
	DM-91	pyrope					m	xenolite		x	x				x	x	x	0.31	>99.5	
	DX-76	almandine			r			rhyolite	Polgárdi, Hungary				x		x	x	x	1.21	~99	
Kyanite	DM-80	light blue - colourless			r		m	schist		x	x				x	x	x	0.93	>99	Qtz
Sillimanite	DM-123	fibrous					p		Pella Steinbock, South Africa	x	x				x	x	x	0.64	~98	weathered to diaspore
Andalusite	DM-75	milky megacryst					p	schist		x	x		x			x	x	0.28	~99	
Staurolite	DM-74	brown megacrystal					m	micaschist	Quimper, Bretagne, France	x	x		x			x	x	0.55	>99.5	with Qtz inclusions
Titanite	A284	brown fragments		a				granodiorite	Ilomantsi, Finland	x	x	x	x			x	x	1.65	~99	
	IVG-8-8	colorless		a				amphibolite	Ivrea body, Southern Alps	x	x	x	x	HNO_3		x	x	0.26	~98	
Olivine	DM-90	light green			r		p	xenolite in basalt		x	x				x	x	x	0.48	>99.5	
Chromite	DM-127	translucent at edges			r		p	ultramafite	Brezovica, Kosovo	x	x	x				x	x	1.16	~98	Mt
Pyroxene	DM-105	aegirine				f	m		Malawi	x	x				x	x	x	0.56	>99	
	DM-6	light green, diopsidic			r		m	diallagite	Pinabasir, Anatolia, Turkey	x	x				x	x	x	0.50	~99	
	DM-124	augite			r		m	xenolite	Paska Pole, Czechia	x	x				x	x	x	0.70	~99	with some biotite incl.
	DX-6B	hypersthene	e		r		p	dacite	Tusnád, Transylvania, Romania	x	x	x	x			x		0.50	~98	with magnetite incl.
Amphibole	DM-69	magnesiohastingsite			r		m		Studsdalen, Kragerø, Norway	x	x	x			x	x	x	0.14	>99.5	
	DM-78	glaucophane-crossite			r	f	p		Pollone Biella, Piemonte, Italy	x	x				x	x	x	0.43	>99.5	
	A993	tremolite-hornblende			r		p	granodiorite	Finland	x	x	x			x	x	x	0.56	>99.5	
	DM-99	hornblende			r		m	xenolite	Ost-Eifel Wehrer Kessel	x	x				x	x	x	0.52	>99.9	
	DM-73	tremolite			r		m		Merelani Hills, Arusha region, Tanzania	x	x				x	x	x	0.68	>99.9	
Epidote gr.	DM-65	green				f	p	vein in basalt	Oman	x	x	x			x	x	x	0.68	>99.9	
	DM-108	clinozoi., light yellow				f	m		Baluchistan, Pakistan	x	x				x	x	x	1.31	>99.5	
	DM-117	dark green				f	m		Region Kayes, Mali	x	x				x	x	x	1.14	>99.9	
	MAU-12	zoisite		a				granitoid	Mauritania	x	x	x				x		0.80	>99.5	
Corundum	DM-102	colourless					m	metamorphites	Madagascar	x						x	x	0.60	>99.9	
Fluorite	WOL1	colourless					m	metamorphites	Wölsendorf, Germany	x						x	x	1.76	>99.9	
Baryte	BU-2	colourless	e	a				limestone	Pál valley quarry, Budapest, Hungary	x	x	x	x	HNO_3		x		0.18	~99	Qtz
Topaz	DM-101	colourless					m	pegmatite	Nigeria	x						x	x	0.72	>99.5	
Cassiterite	DM-81-94	dark + light					m	greisen	Mine San Antonio, La Paz, Bolivia	x	x				x	x		0.80	>99	
Scheelite	DM-128	light yellow					p	granite	Traversella, Piemont, Italy	x	x					x	x	0.92	>99.5	

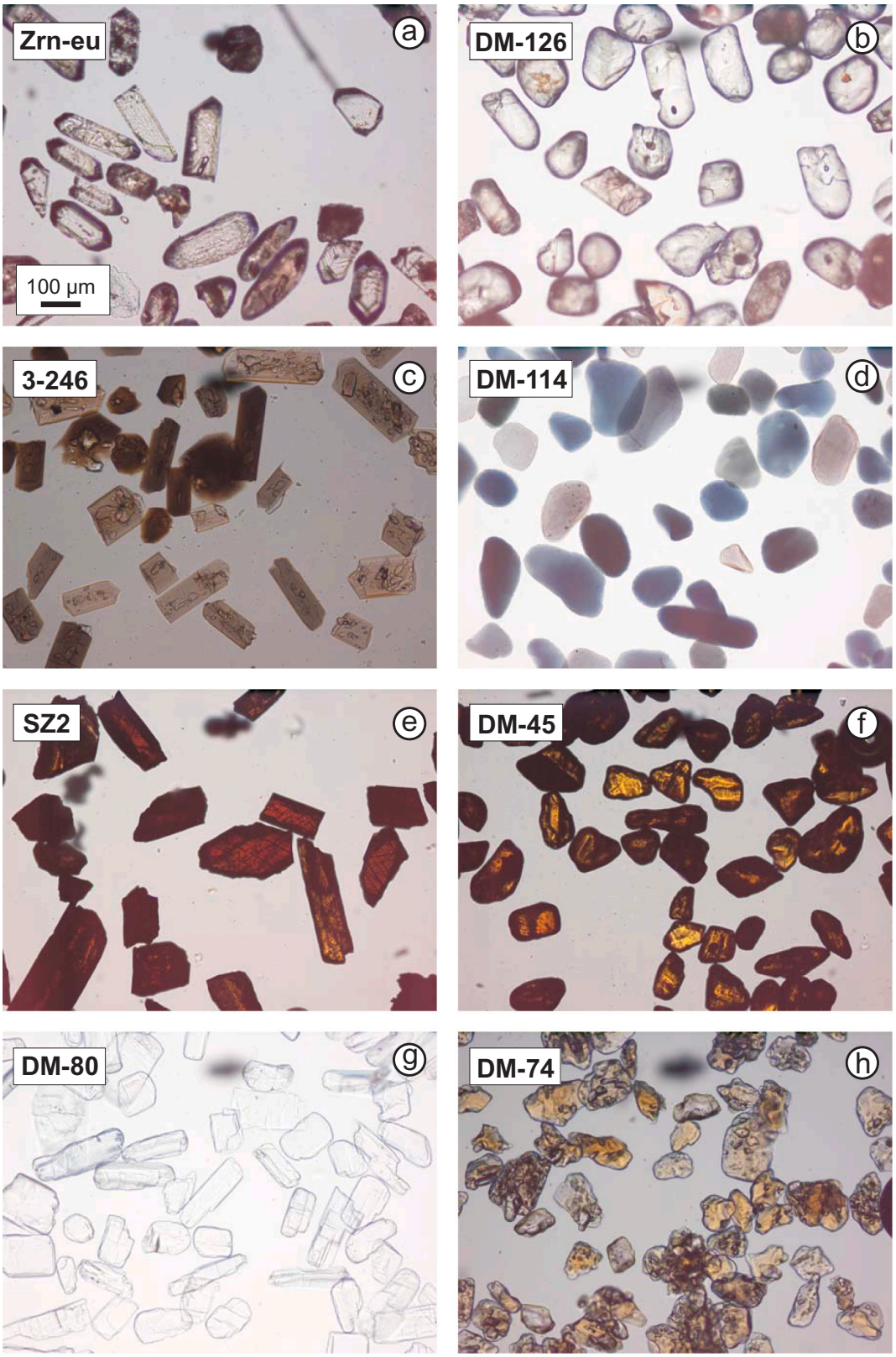

Fig. 1. Microphotographic examples for some mineral samples used for the HMR samples. Polarized light; the width of all images is 1140 µm. The immersion media have a refractive index of n = 1.66. Zrn-eu: Euhedral zircon crystals from granitoids, DM-126: naturally abraded zircon grains from a placer, 3–246: columnar tourmaline crystals with intact prismatic faces, DM-114: air-abraded tourmaline fragments from a several cm-sized crystal from a pegmatite, SZ2: columnar rutile crystals with preserved prismatic faces, DM-45: air-abraded fragments from a big rutile monocryst, DM-80: variably abraded fragments from a kyanite monocryst, DM-74: variable abraded fragments from a staurolite monocryst containing quartz inclusions.

originally designed for U−Pb geochronology (Krogh, 1982). The intensity of the abrasion was varied and aimed at avoiding too well rounded grains without any of the mineral-specific patterns such as cleavage planes. With differently abraded batches from the same mineral samples, variably rounded grain populations were generated.

About 4.5 g mixtures for each HMR sample were generated from the mineral samples by precisely controlled weighing using a 5 digits analytical balance. The HMR-1 and HMR-2 mixtures (Fig. 2) were carefully homogenized and split into 64 aliquots by a micro riffle splitter. Table 1 indicates the gravimetric composition, i.e. weight percentages (wt%) of each of the HMR samples.

3.3. Calculation of nominal grain percentages

Because HM analyses usually provide grain counts, the gravimetric mineral compositions of the HMR-1 and -2 synthetic mixtures are not well-suited for the evaluation of the reported results. The densities of the mineral species are different and despite using a similar sieve fraction the shapes and volumes of the grains for each species differ significantly. The majority of the individual mineral samples were highly pure (typically > 99.5%), but the euhedral apatite and the brookite components contain ca. 15–20% other phases (Table 2) that were considered for the calculation of wt% of the respective phases (Electronic Appendix Table EA 1). Besides density and volume, purity is also considered for the calculations of grain percentages. The principle of the calculation of the nominal grain percentages is described in Appendix B, and Table EA 1 contains the numeric values. The nominal grain percentages are listed along with the weight percentages in Table 1. It is necessary to emphasize that these grain percentages cannot be considered as 'true values'; they can only be considered as an approximation. That is why these concentrations are subsequently called nominal grain percentages or 'nominal values'.

3.4. Distribution of HMR samples and requests to the contributors

The call for the round-robin test was addressed to geoscientists working in the field of provenance analysis of clastic sediments and sedimentary rocks. 242 potential contributors were selected based on a survey of peer-reviewed HM papers in the last ca. 10 years, and they were contacted by e-mails. Further information was provided via a webpage. We outlined the goal of the interlaboratory test round, namely obtaining a reliable image of the variability and comparability of heavy mineral analyses. It was also mentioned that the test was intended to allow for a systematic comparison of results generated by the classical optical HM identification with results obtained by the currently developing automated and semi-automated HM identification techniques.

The contributors were asked to perform the analysis of the HMR samples by the routine methods usually applied in their laboratories, without any special efforts related to these samples. It was also declared that (i) the round robin test did not aim at giving any quality assurance or certificate and (ii) the presentation of the results would be anonymous. Only one of the organizers (I.D.) would know the link between results and contributors. In order to attract many potential participants and to obtain an adequate number of results for statistically robust conclusions, a community-wide common publication was announced, which would be produced with co-authorship of all contributors.

Two types of data were required from the contributors: (i) metadata describing the measurement conditions and (ii) result tables. The metadata should contain the expertise of the observer in three categories, according to the number of HM concentrates measured at the time of analysis as beginner (b, n < 20), advanced user (a, n = 20–50) or experienced user (e, n > 50). In order to obtain another constraint on the activity and experience of the contributors, the number of peer-reviewed papers with their own heavy mineral data was requested. The contributors were further requested to outline their grain mount preparation techniques as applied in the laboratory. In the case of optical mineral identification this includes embedding medium, refractive index, and the counting method (e.g., line counting, ribbon counting, Fleet method, etc.). In the case of automated or semi-automated mineral identification the method and the most relevant settings should be explained.

The submitted result tables should contain the number of all observed grains, number of opaque grains, number of lithic fragments (i.e. composite grains), number of unidentified grains and the remaining number of translucent grains identified (200 was requested as minimum counts). The indication of full mineral names was asked (without abbreviations) and the numbers of detected grains for each mineral species. The organizer did not circulate any template; the contributors were asked to submit the results using their own in-house formats.

4. Methods and results reported by the contributors

We received 73 positive responses, i.e. sample requests, and finally the contributors submitted 65 results, each including both samples, summing up to 130 individual analyses. According to experience, based on the number of analyses performed so far, the contributors are 16 beginners, 12 advanced, and 37 experienced HM analysts. Their publication record ranges from zero to over 100 peer-reviewed papers, which we also classified into three groups (0, 1–3, and > 3 papers).

4.1. Methods applied by contributors

The Electronic Appendix Tables EA 2 (for optical methods), EA 3 (for SEM-EDX techniques) and EA 4 (for Raman methods) contain the laboratory procedures used by the contributors. The method of sample splitting was explicitly requested because sample reduction has a high potential to generate fractionation of the grains according to size, density, shape and surface properties. The laboratories used various techniques, mostly coning and quartering or some kind of micro splitter. However, some used techniques like selection of grains with spatula or spoon or by taking some kind of 'middle fraction' (Table EA 2).

In the optical laboratories, the most commonly used immersion media have refractive indices close to quartz (n = 1.54–1.56), with only few contributors using media with higher refractive indices like 1.59 or 1.66. Various grain-selection methods were used for the scanning of the mounts: line counting, ribbon counting, randomly selected grains by a microscope-stage device (point-counting), the Fleet method, or reducing the latter to specific selected areas. Some optical laboratories used additional methods such as magnetic properties, UV-light, EMP, SEM/EDX or Raman spectroscopy, mostly for selected grains that could not be identified using their optical parameters. In order to increase reproducibility, the positions of the identified grains were routinely archived by photographs or by co-ordinates within the mounts in

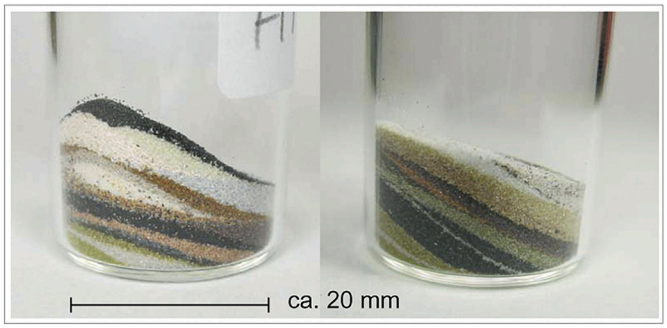

Fig. 2. The HMR-1 (left) and HMR-2 (right) synthetic heavy mineral concentrates before homogenisation.

Table 3

Simplified compilation of the raw grain counting data as submitted by the contributors. Gray background colour indicates mineral species that are summed up into groups marked by black background. The upper part of the table -until the thick line at scheelite- contains the minerals that were added intentionally to the synthetic mixtures. The entire mineral counting data table with comments and the different mineral species identified within the pyroxene-, amphibole- and epidote-groups are presented in the Electronic Appendix Table EA 5 and the percentages and confidence belts in Table EA 6. a) Optical data. b) Electron-beam and Raman spectroscopy data.

	HMR-1, optical mineral identification																																									
code:	O1	O2	O3	O4	O5	O6	O7	O8	O9	O10	O11	O12	O13	O14	O15	O16	O17	O18	O19	O20	O21	O22	O23	O24	O25	O26	O27	O28	O29	O30	O31	O32	O33	O34	O35	O36	O37	O38	O39	O40	O41	O42	O43	O44	O45	O46
Transp. and transluc. heavy m.	202	668	250	303	638	370	338	205	250	239	358	238	292	346	210	551	282	311	200	272	283	317	434	300	211	352	277	1132	201	238	310	321	252	223	254	229	237	199	468	527	337	668	730	1532	1619	305
Zircon	15	45	12	27	70	20	22	11	17	20	34	6	15	18	10	16	27	29	10	24	8	10	36	29	5	13	25	63	18	16	5	12	10	11	10	11	11	33	45	28	8	34	47	58	118	18
Tourmaline	31	95	32		120	50	49	48	46	29	40	33	39	80	18	62	40	35	21	28	60	32	36	46	31	52	56	119	23	28	57	41	31	27	31	27	32	23	58	95	36	84	91	140	188	46
Rutile	23	83	30	10	30	34	36	34	24	26	51	8	35	80	32	74	33	36		30	29	38	53	39	33	39	27	127		30	42	51	28	22	29	22	28	18		59	48	80	88	120	193	33
Anatase		4	7		20				1						7					3	2			7		9	2						12	10	11	10	3						4	7	1
Brookite		1			15	9	6					1						2				1						2					3												
TiO_2 unspecified																			21											32	5			1	2	1									
TiO_2 total	***23***	***88***	***37***	***10***	***65***	***43***	***42***	***34***	***25***	***26***	***51***	***9***	***35***	***80***	***39***	***74***	***33***	***38***	***21***	***33***	***31***	***39***	***53***	***46***	***33***	***48***	***29***	***129***	***32***	***35***	***42***	***51***	***41***	***34***	***41***	***35***	***31***	***18***		***59***	***48***	***80***	***88***	***124***	***200***	***34***
Apatite	17	42	16	31	30	29	26	9	23	7	42	28	16	27	13	9		8	9	22	29	23	25	18	25	24	23	107	5	20	25	17	9	17	9	10	1	17	49	9	15	10	7	44	2	15
Garnet	19	65	22	12	34	40	38	20	32	23	50	37	28	55	30	73	28	30	19	33	35	31	47	25	24	29	25	126	17	18	5	24	25	24	25	24	29	27	117	63	38	64	76	128	67	33
Kyanite	5	58	19	15	45	31	26	8	12	19	6	7	23	23	20	36	24	24	16	20	12	28	41	17	13	35	14	59	16	18		28	18	16	18	16	24			35	26	41	32	50	49	31
Sillimanite	3	31	7			2	1	5	10		13	15	1	2	6	16			1	4	5	24	12	18	2	5	12	16	6		16		11	6	11	7	11			16	12	19	21	35		5
Andalusite		1	4			24	25		1					3		14				3			1					1					5	2	5	6	6				4			24		1
Al_2SiO_5 unspecified																																														
Al_2SiO_5 total	***8***	***90***	***30***	***15***	***45***	***57***	***52***	***13***	***23***	***19***	***19***	***22***	***24***	***28***	***26***	***66***	***24***	***24***	***17***	***27***	***17***	***52***	***54***	***35***	***15***	***40***	***26***	***76***	***22***	***18***	***16***	***28***	***34***	***24***	***34***	***29***	***41***			***51***	***42***	***60***	***53***	***109***	***49***	***37***
Staurolite	21	80	33		35	53	52		32	32		17	29	18	22	74	42	54	31	38	20	31	71	41	44	45	37	200	25	11	11	14	30	27	30	27	23			69	40	104	93	69	99	40
Titanite	2			29	25			3	8	2		13	8	1						10		18	7		1	4		1	0	8						17		23			18	1	10			8
Olivine			3					1		1									24					3				6			12	6	5	3	7	4				15	5	4	11	42		2
Cr-spinel, Mg-chromite	2	12	8							4			7	1	7			3				3		5		13	4	13				15										8				4
Pyroxene total	23	2		93	30	1		25	6	6	60	3		6		12	3	15	1	2	3	1			4				1	7		1	1	1		2	34	25	4	6	5	32	232	194	1
Amphibole total	10	41	22	86	141	38	27	5	6	24	4	5	29	10	16	51	27	16	30	14	8	30	3	14	6	26	12	145	3	11	87	51	10	8	11	9	16	18	61	40	20	42	41	46	59	21
Epidote total	31	102	34		43	30	22	36	25	43	53	27	60	8	25	94	57	59	3	35	67	40	81	34	22	48	31	147	54	65	11	20	50	38	50	48	17	29	90	91	71	153	186	152	519	43
Corundum									1	3			2	1	3	16			14	1	5	7	21																					5	1	1
Fluorite		1																																												
Barite									3			2														7	5							3										4		
Topaz											1													4		3				2						5			3		7	4	46		2
Cassiterite												16		2																			1										10	2	
Scheelite											2									2																	2							26		
No. of "non-added" minerals			1			2			3		2	20		11	1	4	1			3							4		1	1	39	41	6	5	6	5	10					3		287	121	

	HMR-2, optical mineral identification																																										
code:	O1	O2	O3	O4	O5	O6	O7	O8	O9	O10	O11	O12	O13	O14	O15	O16	O17	O18	O19	O20	O21	O22	O23	O24	O25	O26	O27	O28	O29	O30	O31	O32	O33	O34	O35	O36	O37	O38	O39	O40	O41	O42	O43	O44	O45	O46
Transp. and transluc. heavy m.	205	720	250	303	578	402	336	207	275	237	520	233	300	305	200	399	256	257	203	260	252	282	278	310	232	303	318	870	203	204	395	329	270	189	276	202	145	218	278	716	338	528	573	1557	1397	309
Zircon	23	90	27	41	70	31	37	27	28	28	41	17	45	58	32	36	27	23	15	26	12	30	63	34	41	23	52	105	35	37	12	27	19	15	20	16	17	50	49	70	51	57	60	127	121	40
Tourmaline	1	6		5	62	8	4	2			5		1		4			1	6		5		2				47		1	2				1		1		4	28	6	0	4	3		13	4
Rutile	20	35	9	21	15	21	26	19	18	11	45	3	30	53	10	14	24	25		12	18	13	19	13	12	20	27	66		24	45	37	11	10	11	10	9	36	1	31	12	29	18	89	111	26
Anatase											1											1				2								1		1							5	10		
Brookite						4	2	2							5											1																	16			
TiO_2 unspecified																			19										25	1				1												
TiO_2 total	***20***	***35***	***9***	***21***	***15***	***25***	***28***	***21***	***18***	***11***	***46***	***3***	***30***	***53***	***15***	***14***	***24***	***25***	***19***	***12***	***18***	***14***	***19***	***13***	***12***	***23***	***27***	***66***	***25***	***25***	***45***	***37***	***11***	***12***	***11***	***11***	***9***	***36***	***1***	***31***	***12***	***29***	***18***	***110***	***121***	***26***
Apatite	38	91	33	46	115	50	47	25	57	15	88	33	49	3	21	55	25	16	16	41	19	29	25	39	22	43	47	56	5		51	43	41	37	39	28	1	11	39	18	21	16	7	48		39
Garnet	3	24	8	18	22	17	21	13	13	11	21	23	16	11	16	32	7	12	21	10	15	9	5	9	11	6	21	49	9	9	4	3	9	4	8	4	6	23	2	34	8	15	35	88	67	9
Kyanite						4	2		2				9		4			2		2	4					5	1		3	4							3			3	6	15	1		69	
Sillimanite					6				11										13	3	2	3					2										4				4	13	5	21			
Andalusite						35	38		3												2	1				1															2			18			
Al_2SiO_5 unspecified																																														
Al_2SiO_5 total					***6***	***39***	***40***		***16***				***9***		***4***			***2***	***13***	***5***	***8***	***4***					***6***	***3***		***3***	***4***							***7***			***3***	***12***	***28***	***6***	***39***	***69***	
Staurolite					18								1		2	2		9			4						4		9	1							2			1	0		0	23	149	
Titanite	5	83	26	25	10	44	36	17	37	9	32	2	7		9	13	15	6		38	14	11	32	47		14	27	119	7	10	48	46	31	21	31	20	2		13	51	34	52	57	22		33
Olivine	1	3			24	2						4		3		15			17																							2	3	12		
Cr-spinel, Mg-chromite																																2													
Pyroxene total	37	120	51	98	133	22	4	39	41	51	67	52	52	24	40	99	43	32	11	22	26	40	33	32	57	39		119	3	37	60	54	33	27	33	26	34		2	100	104	70	122	339	212	35
Amphibole total	49	87	37	49	55	110	83	35	27	54	132	44	26	47	13	89	65	62	39	39	54	56	11	63	14	45	40	171	35	18	64	65	59	39	58	42	37	47	55	147	29	86	76	188	294	63
Epidote total	27	132	37		48	38	28	27	26	50	81	18	64	99	37	41	42	64	21	52	74	43	53	53	52	60	38	81	69	50	28	13	43	30	47	36	8	47	47	218	44	167	173	170	277	38
Corundum		1	1												6	1	1			1		5		7									3		5	5					9	13		4	3	1	1
Fluorite		6	6							3				3			6	5		1		1		1		2		16			46	7													
Barite		18	5		30			1	4											11				3		12	11	24		9			7	3	5	5									4
Topaz		1	6									1										6		5				32		2			2		5	3	22			28			9	57		13
Cassiterite		3	3							4		10		2			1					34		4	18	24		17					4		6	2						8		27		3
Scheelite		11	1								2									2						2		15					8		8	3						2		33		1
No. of "non-added" minerals	1								8	1	5	26		2	1	2			25		3		35		5	4	1		2		37	32							42			2		271	73	

(*continued on next page*)

Table 3 (*continued*)

	HMR-1, electron beam methods for mineral identification												HMR-1, Raman spectroscopy					
code:	E1	E2	E3	E4	E5	E6	E7	E8	E9	E10	E11	E12	R1	R2	R3	R4	R5	R6
Transp. and transluc. heavy m.	973	454	263	29982	27932	6106	4769	205	324	23891	770	6127	820	210	237	252	1625	200
Zircon	60	24	18	1206	768	210	330	14	22	850	35	303	51	10	10	10	60	6
Tourmaline	210	49	35	4032	3673	653	583	34	38	3159		766	88	17	39	41	180	28
Rutile		58	27		3183	607							103	17	36	42	182	17
Anatase													22	5	3	7	13	3
Brookite		8	5										16	1		2	19	1
TiO_2 unspecified	114			4143			798	30	50	3357	110	832					38	
TiO_2 total	***114***	***66***	***32***	***4143***	***3183***	***607***	***798***	***30***	***50***	***3357***	***110***	***832***	***141***	***23***	***39***	***51***	***252***	***21***
Apatite	80	23	14	1447	850	332	232	11	10	1300	31	303	49	10	15	15	105	10
Garnet	98	39	33	3067	2170	430	509	19	37	2989	71	657	70	17	27	24	196	30
Kyanite		31	15										73	16	21	22	118	13
Sillimanite		35	20										13	8	1	1	10	4
Andalusite													15	4	6	8	45	4
Al_2SiO_5 unspecified	70			3707	3858	787	561	28	37	3330	117	790						
Al_2SiO_5 total	***70***	***66***	***35***	***3707***	***3858***	***787***	***561***	***28***	***37***	***3330***	***117***	***790***	***101***	***28***	***28***	***31***	***173***	***21***
Staurolite	23	46	28	3883	3124	644	371	23	40	2498	62	637	76	45	11	12	213	28
Titanite				4	2	15	1			2	2	3			6			
Olivine	22	11	13	607	343	93	101	2	7	501	17	153	21	6	8	8	41	6
Cr-spinel, Mg-chromite	16	12	6	938	564	427	115	4	10	757	45	148	20				47	6
Pyroxene total				10	8	6	65	3		643		124					2	
Amphibole total	67	32	11	1809	4899	676	225	9	24	968		365	50	17	6	7	52	16
Epidote total	140	81	36	5003	3184	778	863	24	10	3462	110	1026	149	37	43	48	303	27
Corundum	2	2		68	80	11	7				11	19						
Fluorite										7								
Barite				3	100	4	5			2							1	
Topaz	4				348	10				1								
Cassiterite				2	2	1	2			1					3			
Scheelite					1	7				0					1			
No. of "non-added" minerals		3	2	53	11	3	1	4	38	64	159	1	4		1	5		1

	HMR-2, electron beam methods for mineral identification												HMR-2, Raman spectroscopy					
code:	E1	E2	E3	E4	E5	E6	E7	E8	E9	E10	E11	E12	R1	R2	R3	R4	R5	R6
Transp. and transluc. heavy m.	1186	496	322	29165	27250	7258	4681	229	331	18819	725	10797	977	241	210	243	1183	206
Zircon	93	38	35	2410	1236	410	476	24	17	1640	67	54	61	28	21	22	115	15
Tourmaline	1			2	641	41				16			1		2	3	1	
Rutile		21	18		3110	591							37	10	7	8	56	17
Anatase													6	2		1	1	
Brookite													2				2	
TiO_2 unspecified	68			1352			242	14	11	905	25	535					3	
TiO_2 total	***68***	***21***	***18***	***1352***	***3110***	***591***	***242***	***14***	***11***	***905***	***25***	***535***	***45***	***12***	***7***	***9***	***62***	***17***
Apatite	120	63	38	3699	1914	762	587	15	35	2386	114	1570	111	19	30	31	213	32
Garnet	41	13	5	791	1110	288	139	14	6	1077	19	1793	20	13	7	6	36	7
Kyanite																	2	
Sillimanite																		
Andalusite																		
Al_2SiO_5 unspecified	1			8	158	21	1	1		7	11	1						
Al_2SiO_5 total	***1***			***8***	***158***	***21***	***1***	***1***		***7***	***11***	***1***					***2***	
Staurolite				1	86	11				3								
Titanite	115	53	34	3071	1797	648	467	17	44	1997	55	1442	88	25	25	39	121	26
Olivine				1	22	8				5			1					
Cr-spinel, Mg-chromite	1			1	10	286				0	7							
Pyroxene total	42	56	42	8260	332	95	449	58	69	3456		2734	165	46	34	37	186	27
Amphibole total	414	119	64	2019	10907	2177	957	33	86	3230		842	225	49	30	33	140	34
Epidote total	150	83	50	4466	3147	1102	734	30	7	2435	106	544	154	34	32	36	196	30
Corundum	26	17	8	819	726	116	108	2			29	348	22	6	1	3	38	5
Fluorite	13	1		144			64	1	10	387		186	10				11	3
Barite	27	8	1	327	433	90	60	8		191	8	155	14	2	10	10	6	
Topaz	18	8	13	876	462	117	92			529		314	31	4	3	6	30	5
Cassiterite	18	5	9	430	258	59	81	4		264	4	124	12	1			19	1
Scheelite	38	11	5	483	338	116	86	8	6	287		154	17	2	8	8	6	4
No. of "non-added" minerals				5	1		138		38	4	280	1					1	

some laboratories. The time required for the analyses is highly variable ranging from 2 to 35 h.

For the electron beam methods (SEM-EDX) Table EA 3 lists the different analytical techniques, indicates possibilities for grain relocation, additional methods (in this case use of polarizing microscope) and time required for the analysis. The corresponding information for Raman spectroscopic methods can be found in Table EA 4. We do not indicate the type of microscopes and the manufacturer and type of instruments used in the electron beam and Raman laboratories to avoid giving too much information that may allow identification of individual laboratories.

4.2. Reported results

Among the 130 submitted analyses 92 were made by optical grain identification methods, 24 by electron beam based analytical techniques (SEM-EDX), 12 by Raman spectroscopy and two by X-ray diffraction. Table 3 contains a simplified compilation of the grain counts provided by all contributors. The full detailed tables of grain counts and calculated percentages are given in Electronic Appendix Tables EA 5 and EA 6. The appendix tables also contain the details of the identified mineral species within the pyroxene, amphibole and epidote groups as reported by the contributors, while Table 3 shows the total counts of these mineral groups only. As reports of the contributors highly differ regarding identification with the groups, only the total counts of these mineral groups were used for comparison. The number of total transparent and translucent grains measured (N) is highly variable from 145 to 29,982 (Fig. 3). The number of grains identified by the optical method is at maximum around 1600, but mostly between 200 and 400 (74%). The analyses with very high numbers of N were performed by automated electron beam techniques (Fig. 3), although this technique has also been used with relatively low values of N (< 500, 33%). For Raman methods, the numbers are quite similar to the optical methods. All these differences in the total number of transparent and translucent grains indicate that the uncertainties of the concentrations of the components are highly variable and must be calculated individually. The uncertainty estimation is based on Poisson distribution according to the number of identified grains in a component (see explanation in Appendix C). The calculated confidence intervals are listed in Electronic Appendix Table EA 6 and are included in the illustration of measured concentrations for all major components (Fig. 4). This figure provides an overview of the results of the individual analyses and methods in relation to the calculated nominal grain percentages, weight percentages, and the 'best-match averages' (see below).

5. Evaluation and discussion

5.1. Preamble

There are well developed and accepted methods for the evaluation of round robin tests, for instance, the characterization of the spread of the data, the determination of a robust mean or an assigned value and its confidence, as well as methods used for the identification of outliers (ISO/TR 22971, 2005; ISO/IEC 17043, 2010; ASTM Standard D7778, 2012; Szewczak and Bondarzewski, 2016). In most of the round robin tests the individual results have similar uncertainties, and thus it is possible to apply common statistical procedures, calculate simple parameters on the distribution of data and determine scores for the analyses and/or contributors using uniform criteria (e.g., ISO 13528, 2015). This kind of evaluation can be carried out because the analytical procedures measure mostly voltage, current or photon or ion detections in the order of thousands, millions, or even more counts, implying that counting uncertainty has a negligible role. However, in our case the data set is composed of results with strongly variable and mostly low numbers of detections, implying that the measured concentrations have strongly variable uncertainties. It is thus not feasible to assign a *uniform* parameter of 'goodness' to the individual data by just considering their deviation from the nominal concentration or from the mean of the

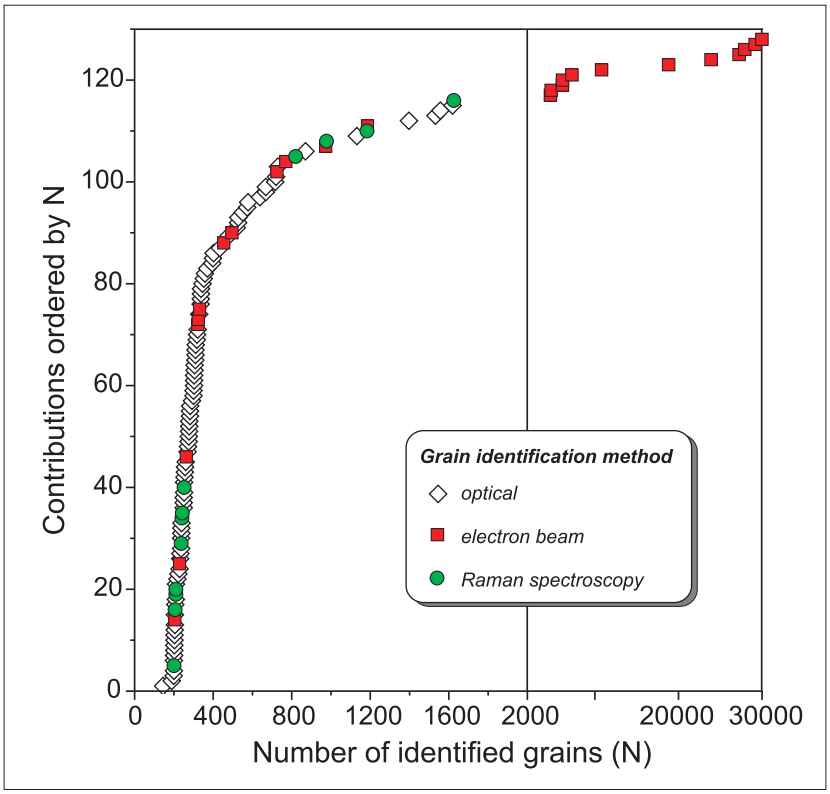

Fig. 3. Cumulative diagram showing the number of reported transparent and translucent heavy mineral grains (N) and the applied methods.

analyses. Such an approach and graphical presentation would be misleading. That is why no confidence belts or circles plotted around the nominal values or averages of the analyses. Instead, the individually calculated (N-dependent) confidence ranges of the reported concentrations compared to the nominal values and to the 'best-match averages' (see below).

Significant control on the spread of the data having low numbers of observations comes from the Poisson uncertainty of the counting statistics. The counting uncertainty is proportional to the reciprocal ratio of the square root of the counts. Appendix Fig. A.2 shows that in the case of low counts the spread of expected values is extremely wide. If we assume a typical number of 200 total transparent and translucent HM counts (N = 200) and assume 1.5% concentration of a given component (like in the case of the minor components), the average number of counts should be 3. In this case 5% of the repeated (and bias-free) measurements will not detect any grain of this component. If the average counted number is 2 then 14% of the analyses should fail and contain zero detection of that given component. This simple estimation implies for the interlaboratory test that we cannot expect the detection of all minor components in all analyses. For evaluation of the results in quantification only the major components are used because the expected spread in the measured concentrations for minor components will be huge according to Poisson statistics.

5.2. Major sources of uncertainty and the spread of the results

Considering the strong influence of the Poisson uncertainty and assuming unbiased sample splitting in the preparation of the HMR aliquots, the total dispersion of the data derives mostly from four sources:

$$\varepsilon_{total} = f(\varepsilon_{GN}, \varepsilon_{FR}, \varepsilon_{MI}, \varepsilon_{count})$$

where.

ε_{GN} = the uncertainty of the number of *grains* of a given component in the HMR aliquot (see Table EA 1)

ε_{FR} = the bias caused by the *fractionation* during sample splitting

ε_{MI} = the bias caused by *mineral mis-identification*

ε_{count} = the Poisson uncertainty based on the number of *counted grains*

Actually only ε_{GN} and ε_{count} can be expressed numerically, and the contributions of the other two sources are unknown. Only in the case of analyses having a large number of identified grains of a given component, the contribution of ε_{count} to the total uncertainty is minor and ε_{MI} can have a high or even dominant role in the observed deviation from the nominal value.

5.3. Comparability and scatter of the results

5.3.1. Graphical evaluation of scatter based on mineral concentrations and ratios

Fig. 4 displays the results for the concentrations of 11 major components of all individual analyses for both samples and all of the four principal methods. It shows (i) an overall significant scatter in the data, (ii) mostly higher scatter for optically obtained data compared to the SEM-EDX and Raman methods (e.g., zircon, apatite, epidote group), (iii) incorrect identification of non-added species, mostly but not exclusively by optical methods (e.g., pyroxene and titanite in HMR-1; Al-silicates, tourmaline and staurolite in HMR-2), and (iv) failure to identify major components in some cases (e.g., tourmaline and staurolite in HMR-1; apatite and titanite in HMR-2).

Because no 'true values' are available (see above), the results are shown in relation to the initially weighted gravimetric percentages, the calculated nominal grain percentages, and the 'best-match averages' (see Section 5.4). The spread of these three values may be taken as a bandwidth of most likely 'true values' (Fig. 4). Relative to this band, some components appear to be measured with largely acceptable precision (e.g., zircon, tourmaline and garnet in HMR-1), while others obviously pose problems in identification and quantification (e.g., staurolite and Al-silicates in HMR-1; amphibole and pyroxene in HMR-2).

Ternary diagrams were used in order to visualize relations in mineral ratios because heavy mineral data are compositional data and the relevant information is always relative (e.g., Tolosana-Delgado, 2012). Fig. 5 shows three ternary diagrams with results for sample HMR-1. The first, zircon–tourmaline–garnet (i.e. the three components showing comparatively small spread in Fig. 4) shows a relatively tight cluster, although some data obtained by optical methods reveal more spread towards a higher zircon proportion. Two analyses did not detect tourmaline. The second, Al-silicates–TiO_2 minerals–epidote diagram shows a similar tight cluster for electron beam (one exception) and Raman methods, but a large spread for optical methods, especially related to epidote proportions. Al-silicates and TiO_2 minerals are not further specified because electron beam methods are not able to detect them (unless combined with other techniques, see Tables 3 and EA 3). The third ternary diagram, zircon–TiO_2 minerals–staurolite shows an overall large spread for all methods, mainly related to staurolite proportions (Fig. 5). Five analyses did not detect any staurolite (all optical), and most of them are additionally biased towards higher zircon proportions.

For HMR-2, the spread in major component analyses is generally higher compared to HMR-1 (Fig. 6). In the ternary diagram pyroxene–amphibole–epidote optical and electron beam methods reveal large contrasts in amphibole/pyroxene ratios, while Raman methods show a relatively small spread. Optical methods reveal additional high spread in epidote proportions, similar to HMR-1. A single electron beam analysis did not distinguish amphibole and pyroxene; that is why only its epidote/chain silicate ratio is presented on Fig. 6. The zircon–apatite–titanite diagram indicates a relatively small spread for electron beam and Raman methods but a large spread for optical methods, mainly towards underestimating titanite proportions and overestimating zircon proportions. Five analyses did not detect any titanite (all optical), and most of them are additionally biased towards higher zircon proportions (Fig. 6).

5.3.2. Evaluation of comparability by mineral indices

From the major components of sample HMR-1 mineral indices (Morton and Hallsworth, 1994; Heroy et al., 2003), a ratio of metamorphic vs. ultrastable minerals and the total percentage of the ultrastable minerals (ZTR: zircon + tourmaline + all TiO_2 phases; Hubert, 1962) were calculated and plotted in order to further assess the scatter in the data (Figs. 7, 8). Sample HMR-2 contains zero or minor proportions of several minerals used for these ratios (tourmaline, rutile, garnet, Al-silicates) and is thus not considered here. With respect to counting uncertainties of the mineral indices, Morton and Hallsworth (1994) suggested to count at least 100 grains per mineral pair. However, for the HMR analyses with total grain numbers mostly between 200 and 500, the numbers of grains for mineral pairs are mostly below this recommendation.

The bar plots clearly illustrate that values and errors of the calculated indices and ratios (further on simply termed indices) vary strongly (Figs. 7, 8). Due to the typically lower number of total grain counts (N) the optical data show the widest error bars, and the smallest ones belong to the automated measurements with high N. The ratios calculated from the nominal grain concentrations and the average of all ratios may

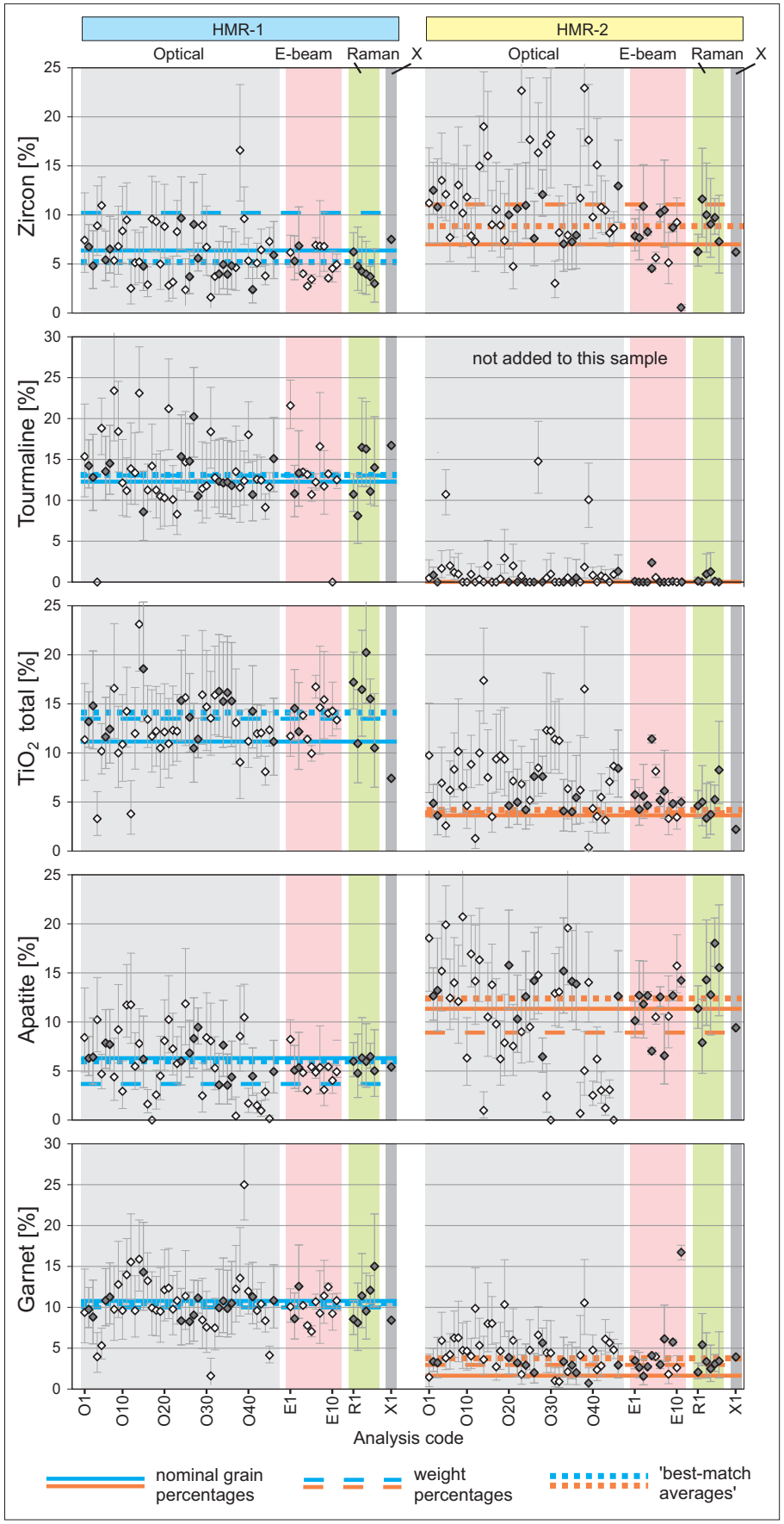

(caption on next page)

Fig. 4. The reported heavy mineral concentrations for 11 major components of the two HMR samples (see details in Table 3 and in the Electronic Appendix Table EA 6). The vertical axes represent grain percentages for the analyses obtained by optical, electron beam and Raman spectroscopic methods, while it represents mass % for the two X-ray diffraction measurements (method X). The blue and orange lines indicate the respective nominal grain percentages (solid), weight percentages (dashed) and 'best-match averages' (dotted). The vertical bars (light gray) represent the upper and lower 95% confidence intervals calculated from the number of identified grains for each analysis. Dark gray symbols represent results considered as belonging to the 'best-match average' (see chapter 5.4). (For interpretation of the references to colour in this figure legend, the reader is referred to the web version of this article.)

be considered as proper reference values. The majority of the 2 s error ranges of the data includes these reference values, but many of the analyses with very low errors obviously miss the reference values.

Table 4 shows the numerical evaluation of the scatter of the indices. The values calculated from the nominal concentrations and the unweighted bulk average from all data are relatively close to each other. However, the differences are partly higher than the standard errors calculated from the reported results (ATi, RZi, ZTR). The relative standard deviations (coefficient of variation) are very high, ranging between 33 and 127%. Calculation of weighted averages is a common procedure when the individual data have variable reliability. However, in our case the application of weighing results in partly significant shifts of the averages away from the nominal value (see ATi and E/G in Table 4). This is largely a consequence of the overvaluation assigned to values generated from data having high N. The MSDW (Mean Square of Weighted Deviates; McIntyre et al., 1966; Wendt and Carl, 1991) is a parameter that offers an estimation of the uncertainties and is widely used, for instance, in geochronology. It is, roughly, *"a measure of the ratio of the observed scatter of the points … to the expected scatter (from the assigned errors and error correlations). If the assigned errors are the only cause of scatter, the MSWD will tend to be near unity. MSWD values much greater than unity generally indicate either underestimated analytical errors, or the presence of non-analytical scatter"* (cited from Ludwig, 2012). Considering all calculated indices and ratios the MSWD values are mostly much above unity (Table 4).

In addition to bar plots the so called 'radial plots' or 'Galbraith plots' are used to evaluate the scatter in the results (Galbraith, 1988, 1990; Vermeesch, 2009; Figs. 7, 8). This is a kind of data presentation that visualizes the uncertainty of the individual analyses and is used for plotting values that have highly variable uncertainties mostly triggered by low counts, like in the case of fission track geochronology and cosmogenic nuclide studies. Radial plots, however, can be readily used for mineral count analyses as well (Vermeesch, 2018). The interpretation of radial plots differs from the commonly used cross plots. The majority of the data having > 10% relative error forms a tight cluster and most of these data plot within the 2 s belt. Some data having much smaller relative error < 5% are loosely scattered and plot well outside the 2 s belt. However, it would be a serious misinterpretation evaluating these data as useless or low quality. Their position is pulled to the right, far from the origin as a consequence of the high counts and associated low error. If we follow their projection lines back, towards the origin (see the example line in Fig. 7, ATi) then it becomes obvious that the calculated indices of the extremely scattered points are not necessarily anomalous and their significance is in line with the majority of the data cluster.

The bar plots, the radial plots and the deduced statistical data highlight the heterogeneity of the data set, which is actually very high and thus common evaluation and comparison of the data is difficult. In order to elucidate the heterogeneity caused by 'low count' and 'high count' data we split the reported results according to the total number of counts (N) into subsets with N < 1000 and N > 1000 (Table 4). The 'low count' subset shows lower MSWD values than the bulk of all data for all the indices, with two indices even close to unity (GZi, RZi). The high-count subset shows higher MSWD values than the bulk of all data. It is crucial to emphasize that this measure does not indicate the 'goodness' of the data, it just shows how reliable the calculated uncertainties are. However, it can also be deduced that in 'high count' data the ε_{count} is low, and the distal positions on the radial plots emphasize the presence of ε_{MI}, while the ε_{MI} remains hidden in the 'low count' subset.

5.4. Estimation of the 'goodness' of the individual measurements

The highly heterogeneous data set obtained by counting of mineral grains is not suitable for use with the common parameters of 'goodness' like z-score or zeta-score (e.g., ISO 13528, 2015). The 'goodness' of the analyses can be assessed only by a pragmatic approach based on the number of detected components and the mistaken detection of 'non-added' minerals (i.e. minerals that have not been added intentionally and may only be present accidentally, in very low amounts due inclusions, contamination, etc.). Such an approach places emphasis on robust presence/absence observations in heavy mineral analysis. In order to express a kind of average of the best measurements we applied the following criteria: (i) all major components must be identified, (ii) at least 6 out of 8 (HMR-2) or 9 (HMR-1) minor components must be identified, and (iii) the percentage of minerals mistakenly identified (i.e. non-added minerals) must be less than 5% (see black frame in Fig. 9). The unweighted arithmetic mean of these results is called 'best-match average'. The number of results considered for the best-match average and their values are listed in Table 5. The selection criteria are justified as follows:

(i) As shown in Figs. 4 and 5 and listed in Table 3 not all major components were identified by all analyses. The detection of the major components is a strong criterion for quality as the approx. 10% (or more) concentration of these components and a minimum value of 200 counted grains would result in 20 counts. In this case the theoretical probability of detecting zero grains is 0.0000002%. Higher grain counts would result in even lower probability of missing a single mineral grain of the component by random sampling. That is why these analyses are distinguished on Fig. 9 and are not considered for the calculation of the best-match average.

(ii) In the case of minor components the probability of zero sampling is relevant (see chapter 5.1), which is why we applied a more tolerant criteria, i.e. identifying at least 6 out of 9 or 8 minor components (for HMR-1 and HMR-2, respectively). Actually this criterion depends on the total number of counted grains, and thus the most accurate approach would be to calculate for each individual analysis the probability of zero counts. This would imply for analyses with N > 2000 (exclusively electron beam methods; Fig. 3), that the identification tolerance for minor components is much stricter. This is not considered to be helpful because the electron beam methods have problems with sample HMR-1, which includes several polymorphs (Al-silicates, TiO_2 minerals) as minor components. For the sake of simplicity the uniform criteria of at least 6 detected minor components was applied for all measurement techniques.

(iii) The proportion of mistakenly identified minerals varies between 0

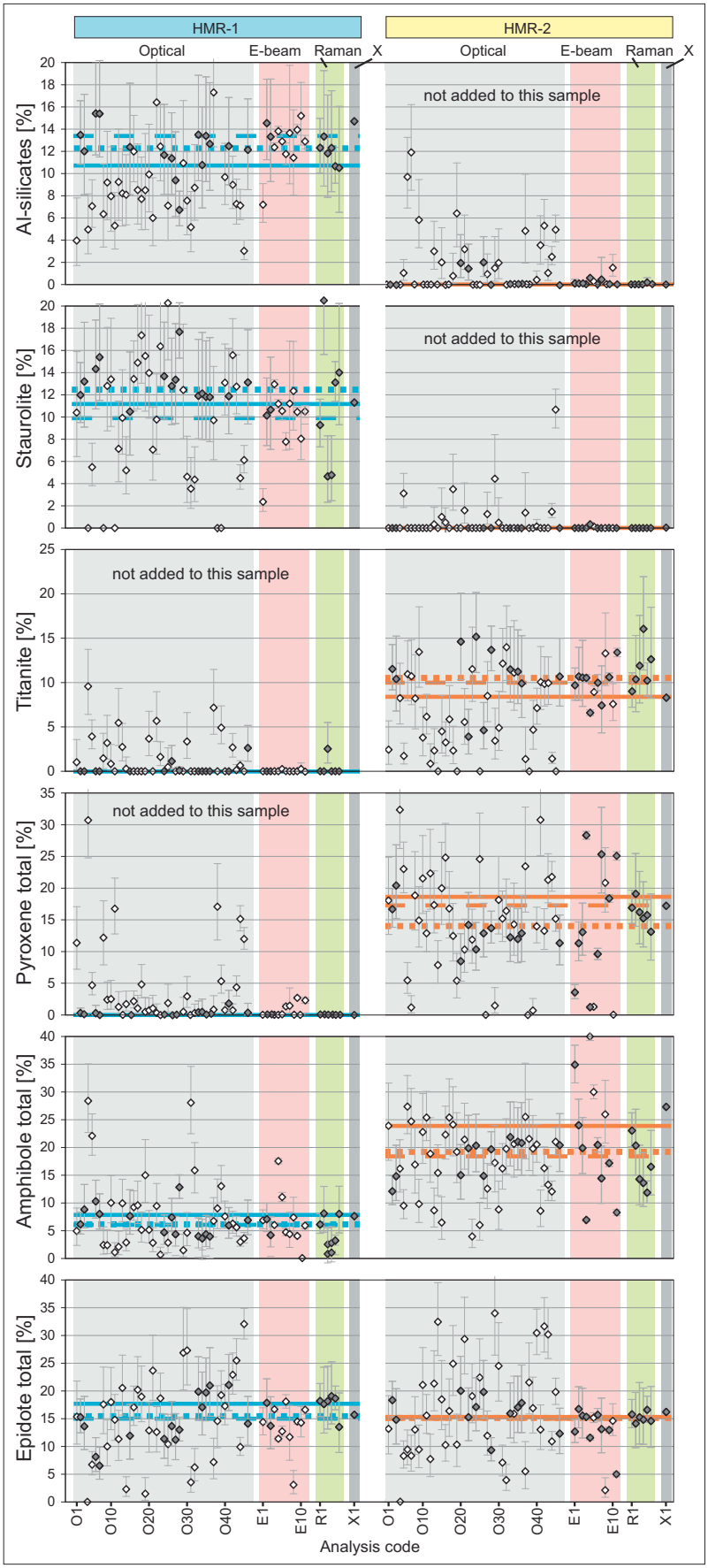

Fig. 4. (*continued*)

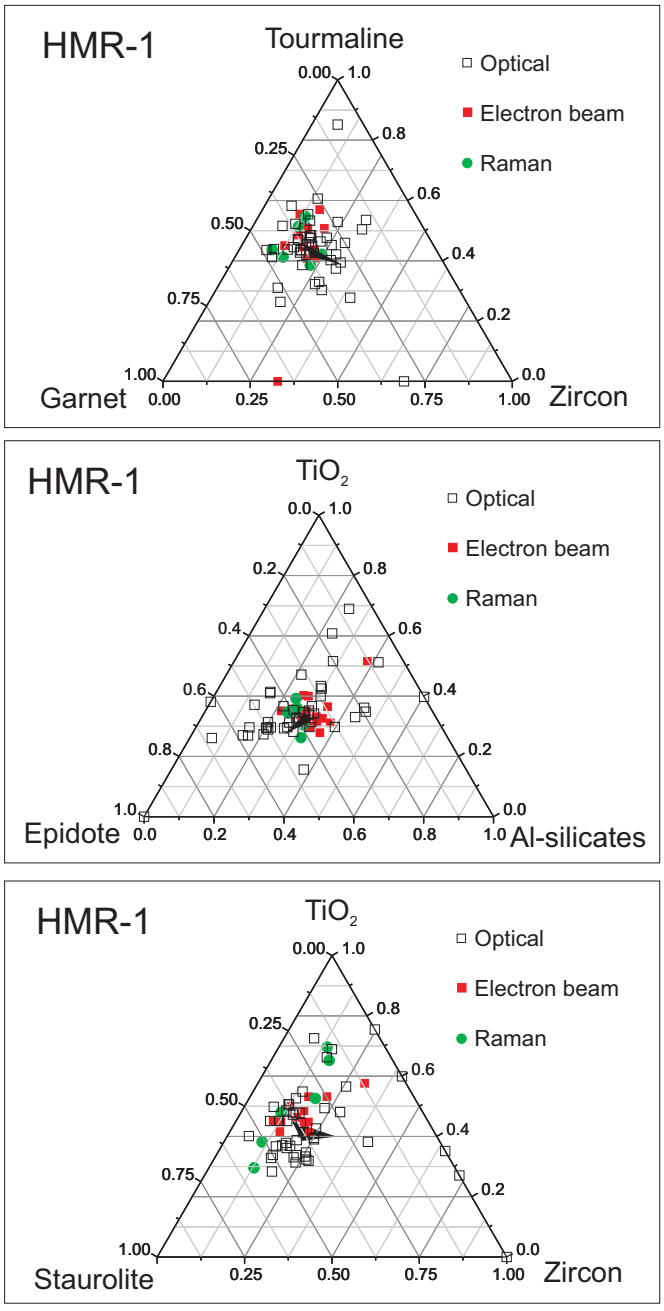

Fig. 5. Ternary diagrams of major components of HMR-1 sample. The black triangles represent the reference compositions between the wt%, nominal grain % and best-match average (see explanation in text).

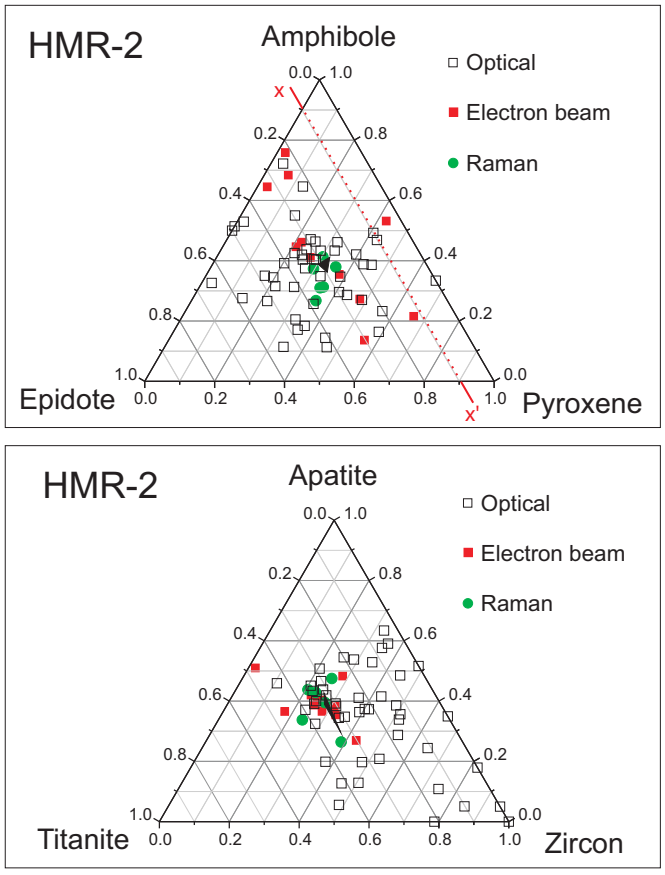

Fig. 6. Ternary diagrams of major components of HMR-2 sample. One electron beam analysis did not distinguish amphibole and pyroxene, thus on the upper diagram this data is shown by a dotted line representing the epidote/(epidote + amphibole + pyroxene) ratio of 0.095.

and 40%. The majority of the mineral samples used for preparation of the HMR synthetic mixtures have high purity (Table 2). However, some heavy minerals that were not added intentionally may be present in the samples. These may come from inclusions or breakdown products like a minor amount of diaspore associated with the quasi-monomineralic sillimanite. The 5% threshold is much higher than possible impurities and contaminations produced during sample preparation according to the characterization (Table 2) and mixing proportion (Table EA 1) of the individual mineral samples.

The different methods contribute in different proportions to the best-match averages. Although the optical analyses provide the highest number for both samples (Table 4), their relative contribution compared to the number of optical analyses is low (15 out of 46 for HMR-1 and 11 out of 46 for HMR-2). In contrast all Raman analyses match the criteria for best-match average (6 out of 6 for both samples). For electron beam methods the relative contribution is low for HMR-1 (2 out of 12) and high for HMR-2 (9 out of 12). The X-ray diffraction analyses are considered for both best-match averages.

5.5. Comparison of the three main methods used for mineral identification

As discussed before the major differences in the uncertainties of the individual analyses derive from the number of the counted grains and we thus have only limited possibilities to estimate the uncertainty derived from bias in mineral identification (ε_{MI}). This problem is tackled in the following by two different approaches.

5.5.1. Comparison of the best-match averages of the different methods

Neither the initially weighted concentrations nor the calculated nominal concentrations (Section 3.3) or the best-match averages (Section 5.4) can be considered as absolute reference level. However, the spread of these values can be taken as a bandwidth of most likely 'true values' (Fig. 4) and their relations may be informative. Fig. 10 shows scatter plots of the best-match averages of the major components

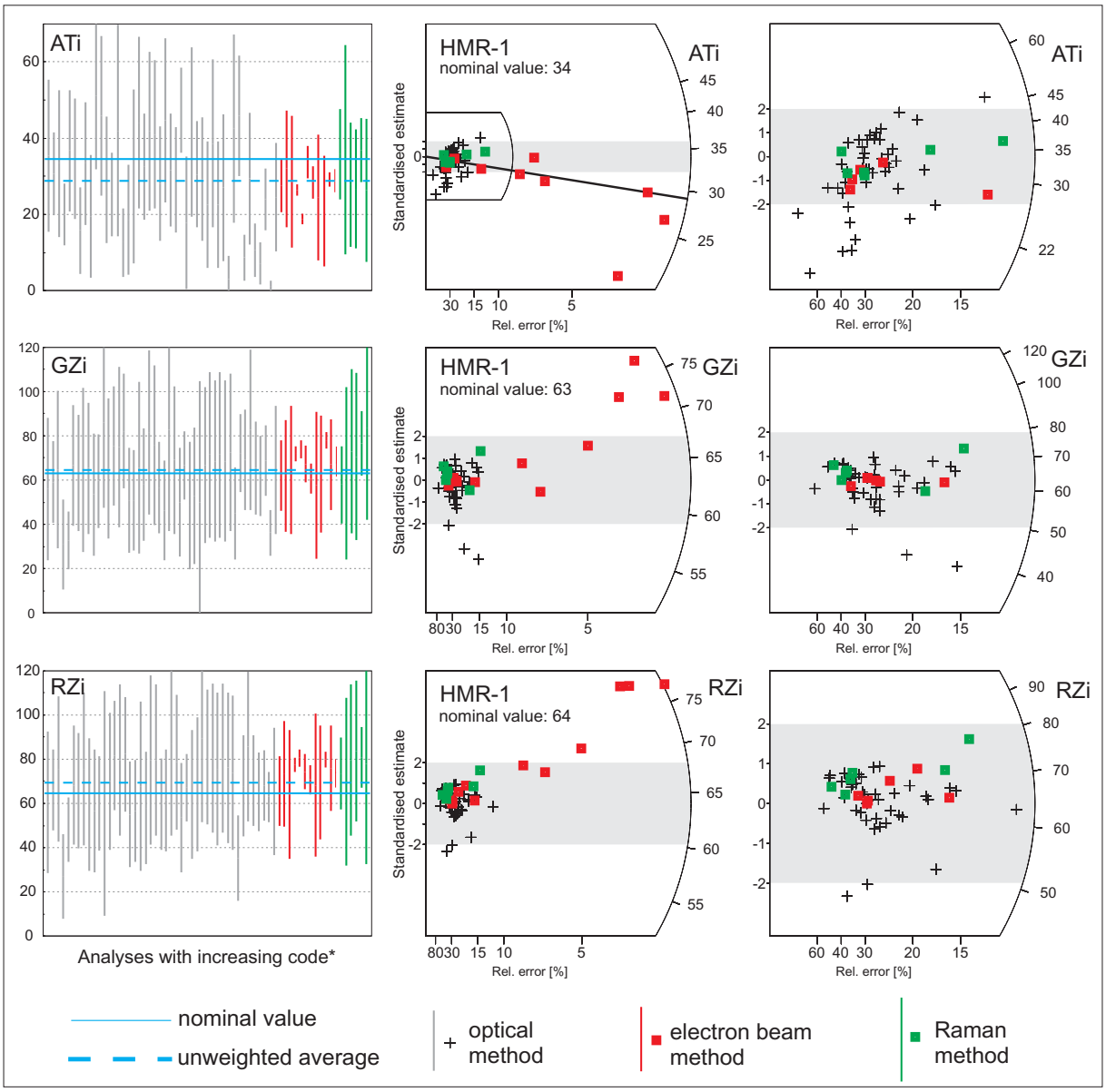

Fig. 7. Provenance-sensitive heavy mineral indices ATi, GZi and RZi (Morton and Hallsworth, 1994) displayed on bar plots and radial plots. The vertical bars represent 2 s error. The right panels are enlarged parts of the dense regions of the radial plots in the middle panels that indicate all data having non zero mineral counts. Radial plots emphasize the error of the calculated value that is controlled by the Poisson uncertainty of the number of counted grains (horizontal axis). The curved scales on the right side of the radial plots indicate the values of the indices. A given measured value can be read on the curved scale by the intersection of a line determined by the origin (0) on the left side and the projection point of the data (see single explanatory line in the top left radial plot). The widths of the gray bands are determined by the scatter of all data generated by the contributors and represent an approx. 95% confidence belt. The X-ray diffraction results can not be evaluated in this way because their uncertainties are not known. **ATi** Apatite Tourmaline index. = 100 * apatite/(apatite + tourmaline), **GZi** Garnet Zircon index. = 100 * garnet/(garnet + zircon), **RZi** Rutile Zircon index. = 100 * all TiO_2 grains/(TiO_2 grains + zircon).
*: The plots contain only the results that recorded the tested major phases.

for each sample and group of methods compared to the nominal concentrations and the weight percentages. The number of data generated is in part rather low, and thus in this plot the spread of the data (1 standard deviation) measured on a given component by one method is presented instead of the error of the mean (standard error).

The data obtained on the HMR-1 sample plot is close to the 1:1 line; the average deviation of the best-match values from the nominal concentrations is 1.5%. The deviations of the individual methods are indistinguishable: 1.7 ± 0.4, 1.3 ± 0.5 and 1.1 ± 0.6% (with ± 1 s.e.) for the optical, electron beam and Raman data, respectively. For this sample the zircon weight percentage and the calculated nominal grain percentage are significantly different. All three methods yielded best-match average zircon concentrations close to the nominal value. This is considered to confirm the reliability of the grain percentage calculation procedure for this sample. For epidote the optical and electron beam best-match average data are closer to the wt% value, but

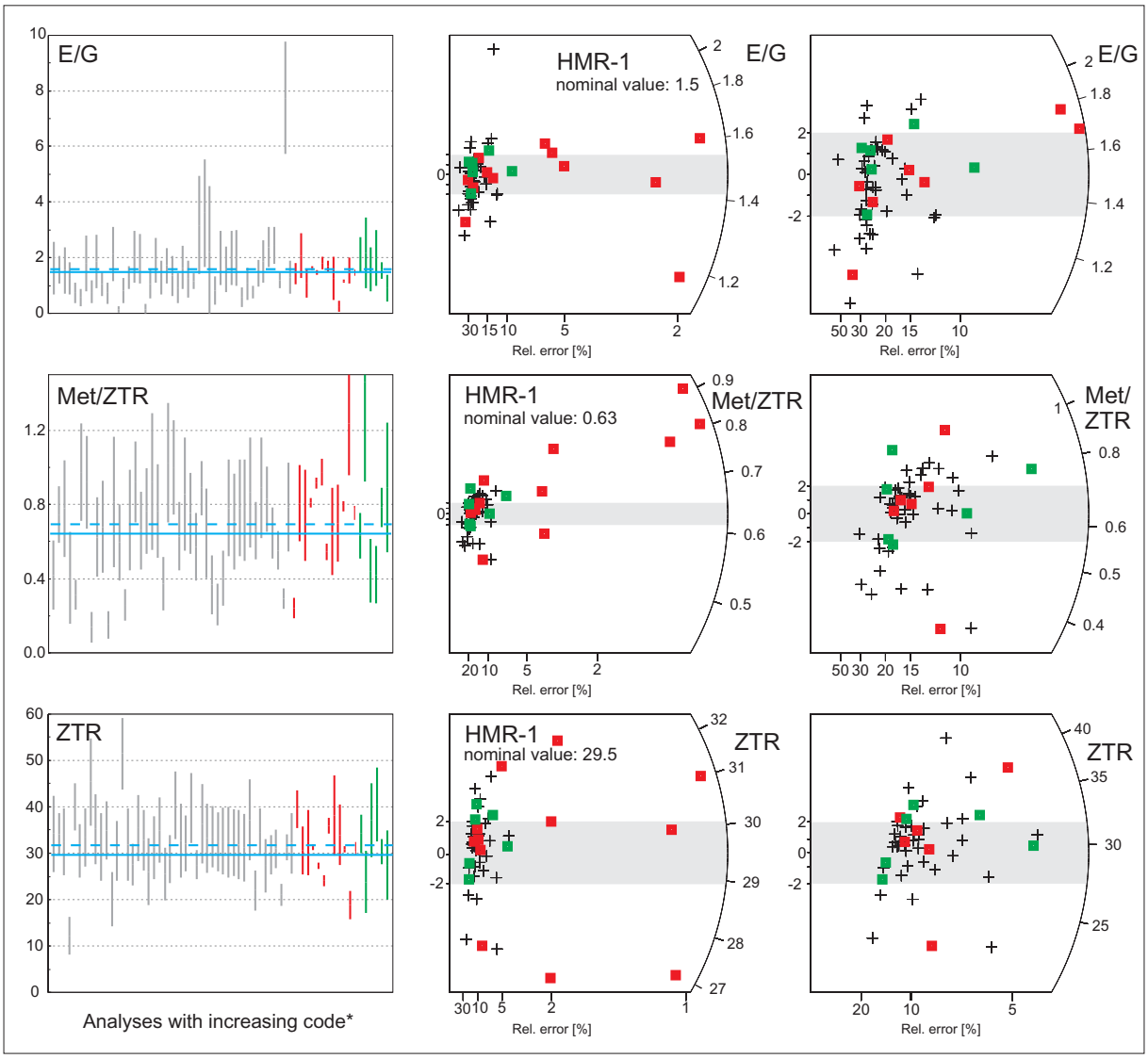

Fig. 8. Epidote/garnet ratio (E/G; Heroy et al., 2003), ratio of metamorphic over ultrastable minerals (Met/ZTR) and the sum of ultrastable heavy minerals (ZTR; Hubert, 1962) displayed on bar plots and radial plots (for explanation see Fig. 7). The sum of all Al-silicates and staurolite as indicative for (para-)metamorphic rocks while the sum of zircon, tourmaline and all TiO_2 phases (ZTR) is considered representative for the ultrastable heavy mineral phases. *: The plots contain only the results that recorded the tested major phases.

for the optical methods the spread is large and for the electron beam methods only 2 analyses are involved in the best-match average.

Sample HMR-2 shows slightly more scatter; the average deviation of the best-match values from nominal concentrations is 2.5%. The deviations of the individual methods are indistinguishable: 3.1 ± 0.8, 1.9 ± 0.5 and 2.9 ± 1.0% for the optical, electron beam and Raman data, respectively. For apatite and epidote all three methods show a good fit. In the case of amphibole and pyroxene most best-match averages are below but close to the nominal values while all wt% are above nominal values. The large spread in amphibole and pyroxene for electron beam methods results from problems in distinguishing these phases (Fig. 10).

This comparison shows that, considering the best-match averages only, the data are quite reasonable and do not show systematic deviations from the 1:1 line (see Fig. 10). This holds for both samples and all of the three methods. However, the scatter is sometimes quite high (e.g., epidote and pyroxene for optical methods, amphibole and pyroxene for electron beam methods, staurolite and amphibole for Raman methods).

5.5.2. Comparison of the methods by the number of major component concentrations matching the reference values

The quality of the analyses is further evaluated by the number of major components that match the reference values within 2 s confidence range. This assessment has been performed using all data and both the nominal concentration and the best-match averages as reference values (Fig. 11). Results are remarkably similar and independent of the reference values used.

The proportion of major components within the 2 s confidence range is on average higher for sample HMR-1 compared to HMR-2 (4.6 out of 7 vs. 3.1 out of 6, respectively; Fig. 11). This contrast is most likely due to the composition of the samples. HMR-1 contains more

Table 4
Evaluation of some statistical parameters obtained on the mineral indices calculated from HMR-1 results.

	ATi	GZi	RZi	E/G	Met/ZTR	ZTR [%]
Nominal	34	63	64	1.50	0.63	29.5
n	61	64	63	63	62	64
Average	28.9	64.2	69.5	1.58	0.69	31.9
2 s.e.	*2.8*	*2.9*	*2.9*	*0.3*	*0.1*	*1.5*
2 r.s.d.	*75%*	*36%*	*33%*	*127%*	*72%*	*38%*
Weighted aver.	19.3	68.7	74.8	1.19	0.68	29.5
MSWD	**19**	**2.5**	**1.8**	**17**	**29**	**9.5**

	ATi	GZi	RZi	E/G	Met/ZTR	ZTR [%]
	Using data only with Ntotal < 1000					
n	52	55	54	54	53	55
Average	27.1	63.8	68.8	1.49	0.68	31.3
2 r.s.d.	*94%*	*37%*	*35%*	*92%*	*76%*	*55%*
Weighted aver.	21.3	59.7	65.3	0.73	0.45	30.7
MSWD	**3.8**	**1.0**	**1.06**	**8.9**	**11**	**5.8**

	ATi	GZi	RZi	E/G	Met/ZTR	ZTR [%]
	Using data only with Ntotal > 1000					
n	9	9	9	9	9	9
Average	27.3	66.6	66.6	2.16	0.73	28.8
2 r.s.d.	*88%*	*38%*	*38%*	*195%*	*60%*	*31%*
Weighted aver.	18.9	71.4	71.4	1.39	0.77	29.3
MSWD	**103**	**8.0**	**8.0**	**21**	**63**	**31**

The MSWD values are emphasized by bold typing as in our context they are more important than the averages calculated by different methods. ATi, GZi and RZi are apatite-tourmaline, garnet-zircon and TiO_2-zircon indices, respectively (Morton and Hallsworth, 1994).
E/G and Met/ZTR are the epidote/garnet and metamorphic HM/ZTR ratios. where Met = Al-silicates + staurolite, ZTR = zircon + tourmaline + all TiO_2 (ultrastable assemblage).
ZTR [%] = percentage of ZTR.
n: number of analyses that contain data for the calculation of indices or ratios.
Nominal: indices or ratios calculated from the nominal percentages of the HMR-1 sample.
Average: unweighted arithmetic mean of the calculated indices/ratios.
MSWD: Mean Square of Weighted Deviates, see text for details.
n.c.: not calculated (as the 'external error' was not detectable).

'common' heavy minerals like zircon, tourmaline, rutile, garnet and Al-silicates, typical for provenance from metamorphic rocks, while major components of HMR-2 were dominated by chain silicates, epidote, and titanite (see Section 3.1), whose recognition and discrimination were less accurate (Fig. 6).

Considering the methods, the majority of the optical analyses yields a high proportion of matching results for HMR-1, mostly between 4 and 7 out of 7. Proportions for HMR-2 are significantly lower, mostly peaking in the mid-range, i.e. 2–4 out of 6 (Fig. 11). The data generated by Raman spectroscopy have the highest proportions of matches, roughly similar to the optical methods for HMR-1, and better than all the others for HMR-2. The electron beam analyses are evenly distributed with a significant part of low matching results. Again, this comes from the low counting statistical error for analyses with high totals (N), implying smaller confidence belts. Due to this methodological bias, average method-specific results for major component concentrations cannot be compared satisfactorily.

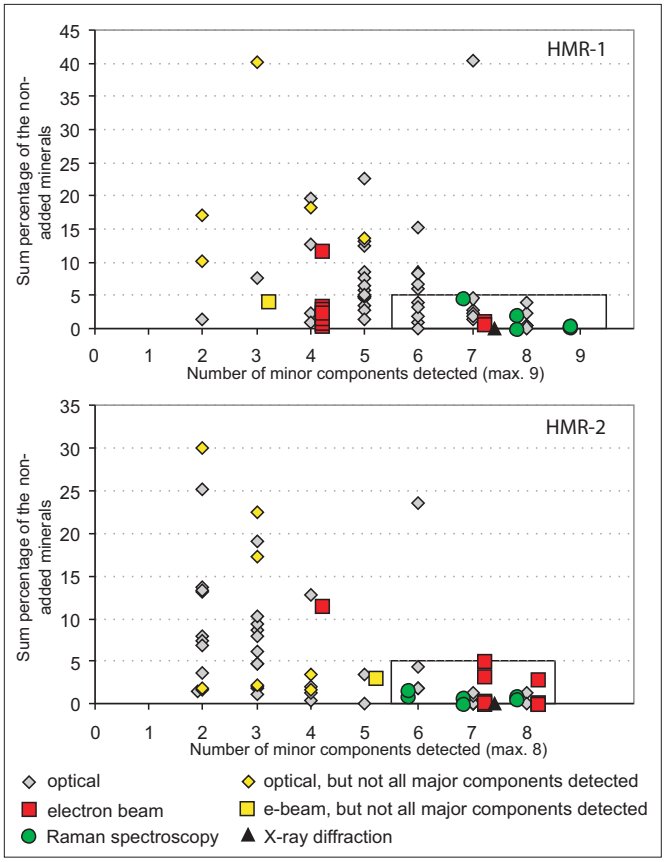

Fig. 9. Estimation of the 'goodness' of the analyses derived from the number of trace components identified and the sum of minerals detected in the HMR samples, that were not added intentionally (i.e. 'non-added minerals'; see details in Electronic Appendix Table EA 6). Black frames comprise the data that contain less than 5% non-added minerals and more than 5 identified minor components. These analyses are used to calculate the 'best-match average'.

5.6. The potential influence of the individual experience of the contributors

Experienced analysts are expected to produce overall better results. As a measure for experience two criteria were used, the number of HM samples quantified at the time of analysis and the number of peer-reviewed papers with the analysts' own heavy mineral data (Section 3.4). The response is evaluated with respect to (i) the average deviation of measured major component percentages from the nominal grain percentage composition of the samples (Table 6), and (ii) the measured individual proportions of major components depending on experience, illustrated in ternary diagrams (Fig. 12). The average deviation in major component quantification reveals smallest numbers for the experienced researchers, independent of criteria (Table 6). However, results are significant for sample HMR-1 only. For HMR-2 the contrasts are insignificant; all average values are similar within error. Looking at individual mineral proportions for the latter sample (Fig. 12), amphibole/pyroxene ratios are highly variable, independent of experience. The high spread in epidote proportions and the tendency to overestimate zircon proportions using optical methods (Section 5.3.1; Fig. 6) is less pronounced for experienced scientists with > 3 publications. These operators also did not fail in the identification of titanite and their data show less spread in titanite proportions (Fig. 12). In essence, experience

Table 5
Evaluation of the averaged results according to mineral species. Bold-Italics numbers are the major components. n: number of analyses considered for best-match averages (see text for explanation).

	HMR-1							HMR-2						
	wt%	Nominal	Best-match average					wt%	Nominal	Best-match average				
			All		O	E	R			all		O	E	R
		n:	24		15	2	6		n:	27		11	9	6
			Average	s.d.	Average	Average	Average			Average	s.d.	Average	Average	Average
Component	[%]	[%]	[%]	[%]	[%]	[%]	[%]	[%]	[%]	[%]	[%]	[%]	[%]	[%]
Zircon	***10.2***	***6.3***	***5.2***	***1.7***	***5.5***	***6.1***	***4.3***	***11.1***	***6.9***	***8.9***	***2.7***	***10.0***	***7.7***	***9.0***
Tourmaline	***13.0***	***12.2***	***13.0***	***2.7***	***13.2***	***12.1***	***12.8***			0.3	0.6	0.2	0.3	0.4
Rutile	10.2	9.1	11.6	2.2	11.4	11.5	12.0	4.0	3.7	4.1	2.9	5.2	2.4	4.6
Anatase	2.0	1.3	1.8	1.7	2.0	0.0	1.9			0.1	0.3	0.1	0.0	0.3
Brookite	1.3	0.7	0.6	0.8	0.4	1.8	0.8			0.0	0.1	0.0	0.0	0.1
TiO_2 unspecified			0.2	0.5	0.1	0.0	0.4			1.2	2.3	0.0	3.5	0.0
TiO2 total	***13.5***	***11.1***	***14.2***	***2.6***	***14.0***	***13.4***	***15.1***	4.0	3.7	5.5	1.8	5.4	5.9	5.0
Apatite	3.7	6.3	6.0	1.5	6.2	5.2	5.7	***8.9***	***11.4***	***12.4***	***2.9***	***12.8***	***11.2***	***13.3***
Garnet	***10.0***	***10.8***	***10.5***	***1.8***	***10.3***	***10.6***	***10.8***	3.0	1.7	3.9	2.9	3.2	5.1	3.3
Kyanite	7.9	6.1	7.6	1.4	7.6	6.3	8.0			0.1	0.4	0.2	0.0	0.0
Sillimanite	3.4	2.3	3.0	2.2	2.9	7.7	1.5			0.2	0.4	0.4	0.0	0.0
Andalusite	2.0	2.3	1.7	2.0	1.6	0.0	2.4			0.2	0.5	0.4	0.0	0.0
Al_2SiO_5 unspecified			0.0	0.0	0.0	0.0	0.0			0.3	0.8	0.5	0.1	0.0
Al_2SiO_5 total	***13.3***	***10.7***	***12.2***	***1.9***	***12.2***	***13.9***	***11.8***			0.3	0.6	0.5	0.1	0.0
Staurolite	***9.9***	***11.2***	***12.3***	***3.5***	***13.0***	***10.4***	***11.2***			0.0	0.1	0.0	0.0	0.0
Titanite			0.3	0.8	0.3	0.0	0.4	***9.9***	***8.4***	***10.6***	***2.8***	***10.7***	***9.9***	***11.7***
Olivine	2.0	2.3	1.6	1.4	0.8	3.7	2.9			0.0	0.1	0.0	0.0	0.0
Cr-spinel, Mg-chromite	3.0	3.5	1.4	1.3	1.3	2.5	1.4			0.0	0.0	0.0	0.0	0.0
Pyroxene total			0.2	0.4	0.2	0.0	0.0	***17.2***	***18.7***	***14.5***	***6.1***	***13.2***	***15.1***	***16.0***
Amphibole total	6.1	7.9	6.1	2.6	6.6	5.6	5.1	***18.3***	***23.9***	***18.7***	***7.1***	***18.2***	***20.6***	***16.6***
Epidote total	***15.0***	***17.7***	***15.4***	***4.0***	***14.5***	***15.8***	***17.5***	***15.0***	***15.3***	***14.9***	***3.2***	***16.2***	***13.2***	***15.2***
Corundum			0.1	0.3	0.1	0.2	0.0	2.0	2.5	1.6	1.1	1.0	2.2	2.0
Fluorite			0.0	0.0	0.0	0.0	0.0	2.0	1.7	0.7	0.7	0.6	0.8	0.6
Baryte			0.2	0.6	0.3	0.0	0.0	2.0	0.7	1.9	1.3	2.2	1.6	1.9
Topaz			0.1	0.3	0.2	0.0	0.0	2.0	2.8	2.0	1.2	1.7	2.2	2.3
Cassiterite			0.1	0.3	0.0	0.0	0.2	2.0	1.0	1.8	2.6	2.8	1.5	0.6
Scheelite			0.0	0.1	0.0	0.0	0.1	2.0	1.2	1.7	1.1	1.2	2.0	2.0

helps to improve the quality of analyses obtained by optical methods, although the effect appears to be smaller than expected. Such a small effect is supported by the proportions of analyses obtained by beginners, advanced and experienced users included in the best-match averages, which are 9 out of 32 (28%), 11 out of 24 (46%) and 32 out of 74 (43%), respectively (integrated over all methods).

5.7. The potential influence from using different methods of sample splitting and counting

Careless sample splitting is considered as a major source of error in HM preparation (Section 2.3). Three different techniques can be compared based on the reported data: coning and quartering, micro splitter and 'other methods', the latter summarizing a variety of different techniques (Section 4.1; Table EA 2). The results suggest only a minor effect of the splitting method. Coning and quartering yield slightly better average values for both samples, while 'other methods' yield slightly poorer results (Table 7).

Different counting methods were used and their effect on HM analyses is debated, especially regarding grain-size effects (Section 2.4). The comparison of the three most-used techniques reveals the lowest average deviation for the Fleet method and highest average deviation for line counting, for both samples (Table 8). Note that some modifications of the Fleet method, such as counting all grains within selected areas of the slide, were included in this group. The results for the most frequently used ribbon counting method is in between the two other methods.

6. Conclusions and suggestions

(1) The standard procedures used for comparison of data from inter-laboratory tests are not applicable in this study, mainly due to the huge spread in number of counts and associated Poisson counting statistics. For estimating the 'goodness' of the analyses and extracting a reliable mean value from the data (the 'best-match average') we applied pragmatic and robust criteria, based on the number of correctly identified components and the total percentage of mis-identified minerals that were not present (i.e. 'non-added').

(2) Given the high Poisson counting errors for the bulk of the samples with $200 < N < 500$, the overall comparability is reasonable. However, there are some problems with respect to a number of laboratories and/or operators, which are partly related to the methods used. These include:
- Optical methods yield the overall poorest results with respect to the scatter of the data. This, however, seems to be rather a problem of the operators and cannot be considered inherent to the method as demonstrated by a significant number of optical analyses which match the criteria of the 'best-match average' (26 out of 92). The main problems of several operators include (i) non-detection of major components, which is considered very critical,

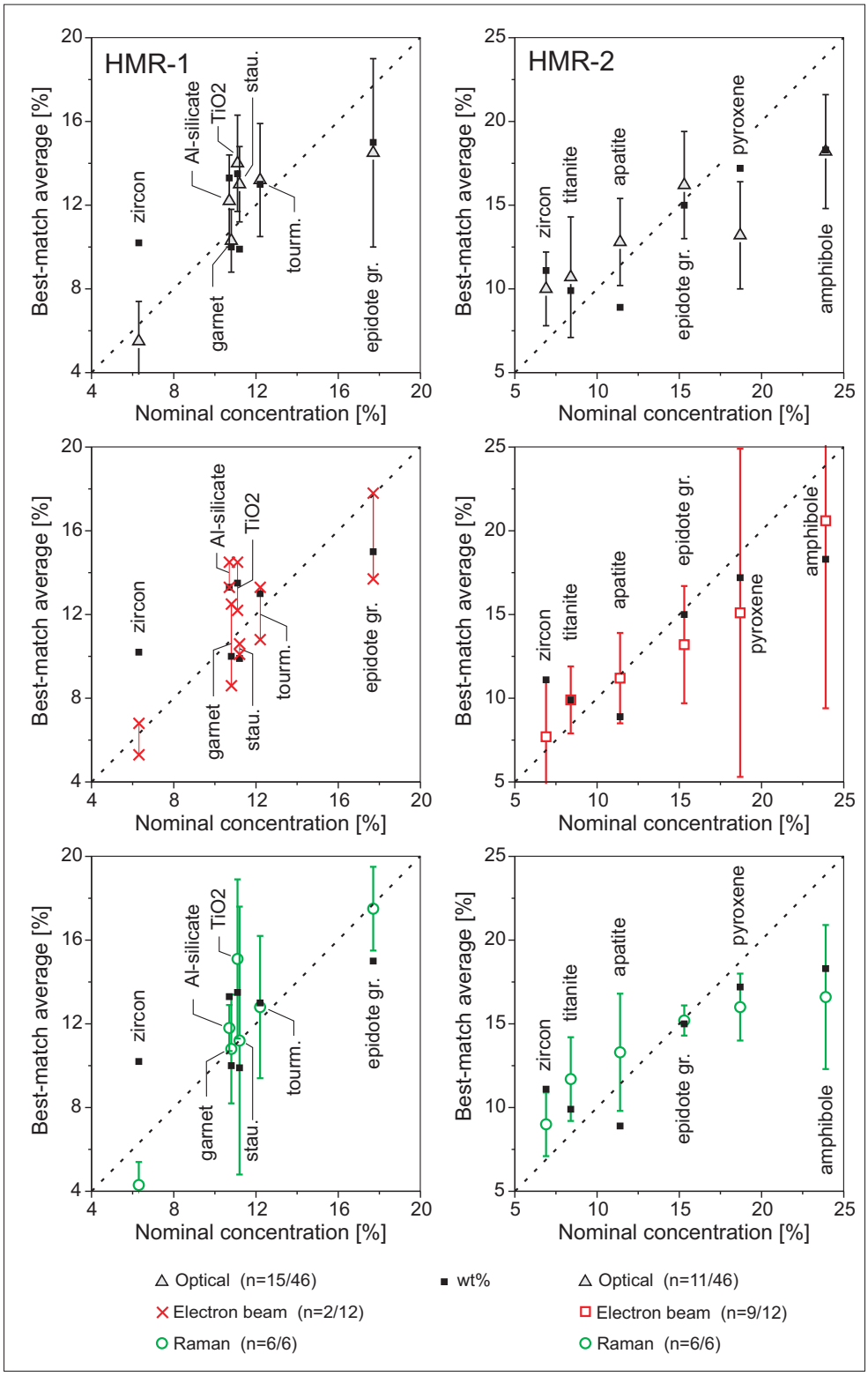

Fig. 10. Relation of the calculated nominal concentrations vs. the best-match averages for the major components of sample HMR-1 (left) and HMR-2 (right), separated for the three main methods. Bars represent 1 s standard deviation. Initial weight percentage concentrations are also indicated. In sample HMR-1 the electron beam method is represented only by 2 analyses, thus the individual data are plotted and not averages.

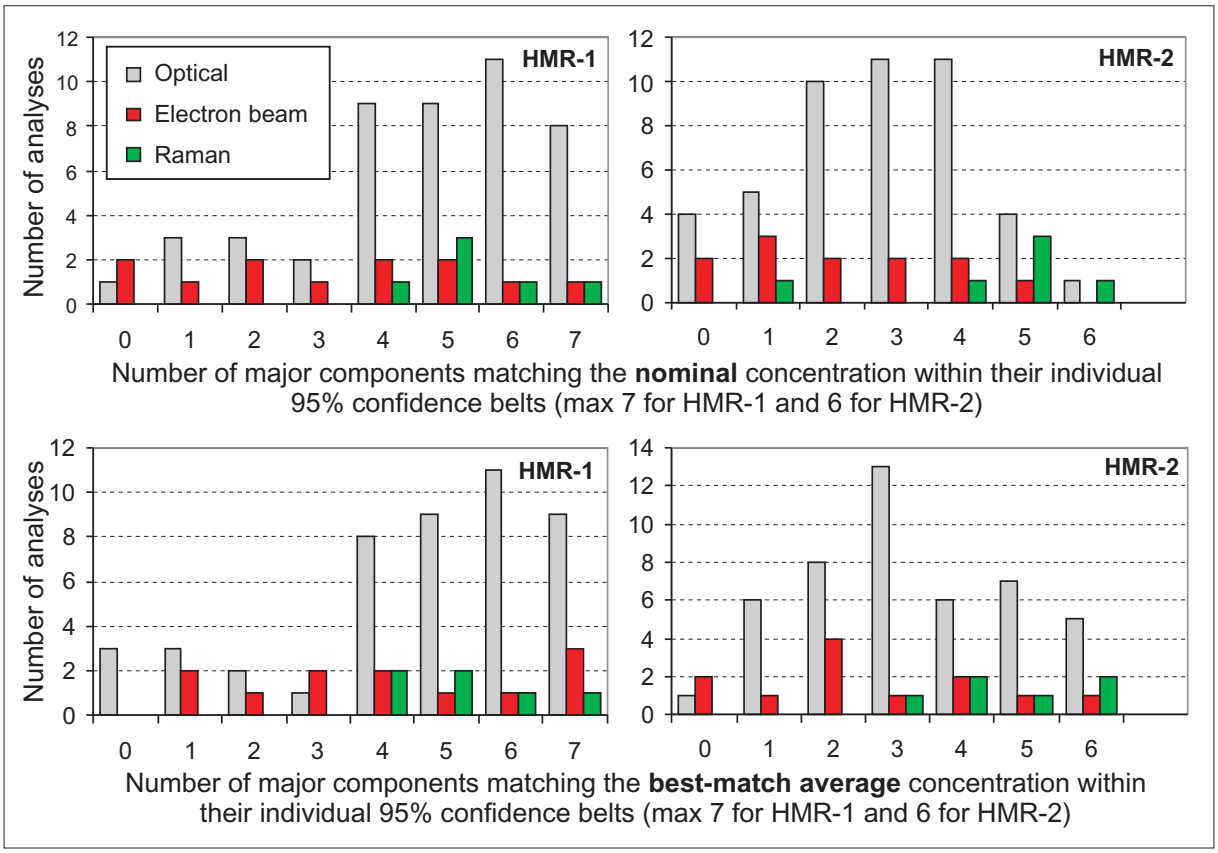

Fig. 11. Estimation of the 'goodness' of the analyses according to the deviation of the concentrations of the major components from the nominal concentrations and from the best-match average concentrations (see details in Electronic Appendix Table EA 6). The X-ray diffraction results can not be evaluated in this way as the uncertainties of the concentrations are not known.

and (ii) a considerable number of minerals being incorrectly detected at high proportions (up to 40%), which were not added to the HMR samples.

- Electron beam methods (SEM-EDX) yield overall satisfactory results, although only 46% (11 out of 24) matched the criteria for 'best-match average'. This is mostly due to the high proportion of polymorphs in sample HMR-1. Another difficulty seems to be related to the discrimination of chain silicates, e.g., various types of amphiboles and pyroxenes. Partly because of the very high number of counts, the ensuing small individual counting errors often result in some offset from the nominal and average values or calculated indices. This effect should not be overvalued because it simply results from mistakes in mineral identification, which are otherwise masked by the high counting errors.
- Raman methods yield very good results with respect to the criteria for 'best-match average', which was satisfied by all analyses (12 out of 12). Similarly, the best results were obtained for the number of major components quantified within 95% confidence. However, some analyses reveal problems with mineral identification, mainly related to staurolite, titanite, and TiO_2 minerals.

(3) The contributors were requested to use the methods of sample preparation and counting routinely applied in their laboratories. Comparison of the data obtained by optical methods (the largest group of analyses) reveals the best results for coning and quartering during sample splitting although contrasts are small. The Fleet method (and modifications used by the contributors) appears to be more robust than other methods, especially line counting.

(4) Experienced researchers obtained overall better results in optical identification. The effect, however, must be considered minor, especially with respect to the more complex sample HMR-2, where even some experienced users missed major components.

(5) Only one laboratory used the X-ray diffraction technique, and the results were reported with unknown errors. Therefore, the method could not be included in any of the statistical comparisons. The comparison to the exactly determined weight percentages of the HMR samples indicate the results were accurate.

(6) The study was designed to evaluate overall determination of heavy mineral assemblages. For associated studies such as mineral chemistry or geochronology, the study of mineral alteration and corrosion, or the study of silt-sized materials, the different heavy mineral methods have their specific advantages and disadvantages, which are not considered here.

Table 6
Average absolute deviation of major component grain percentages from the nominal composition of the samples in [%] vs. experience of the contributors, classified in three categories.

	No. of HM analyses performed at the time of the test		
	< 20 (16)	20–50 (12)	> 50 (37)
HMR-1	4.2 ± 0.6	3.2 ± 0.5	2.6 ± 0.2
HMR-2	5.7 ± 0.7	5.1 ± 0.8	4.9 ± 0.3

	No. of peer-review publications with own HM data		
	0 (24)	1–3 (19)	> 3 (21)
HMR-1	3.2 ± 0.3	3.5 ± 0.4	2.8 ± 0.3
HMR-2	5.2 ± 0.5	5.5 ± 0.5	4.9 ± 0.4

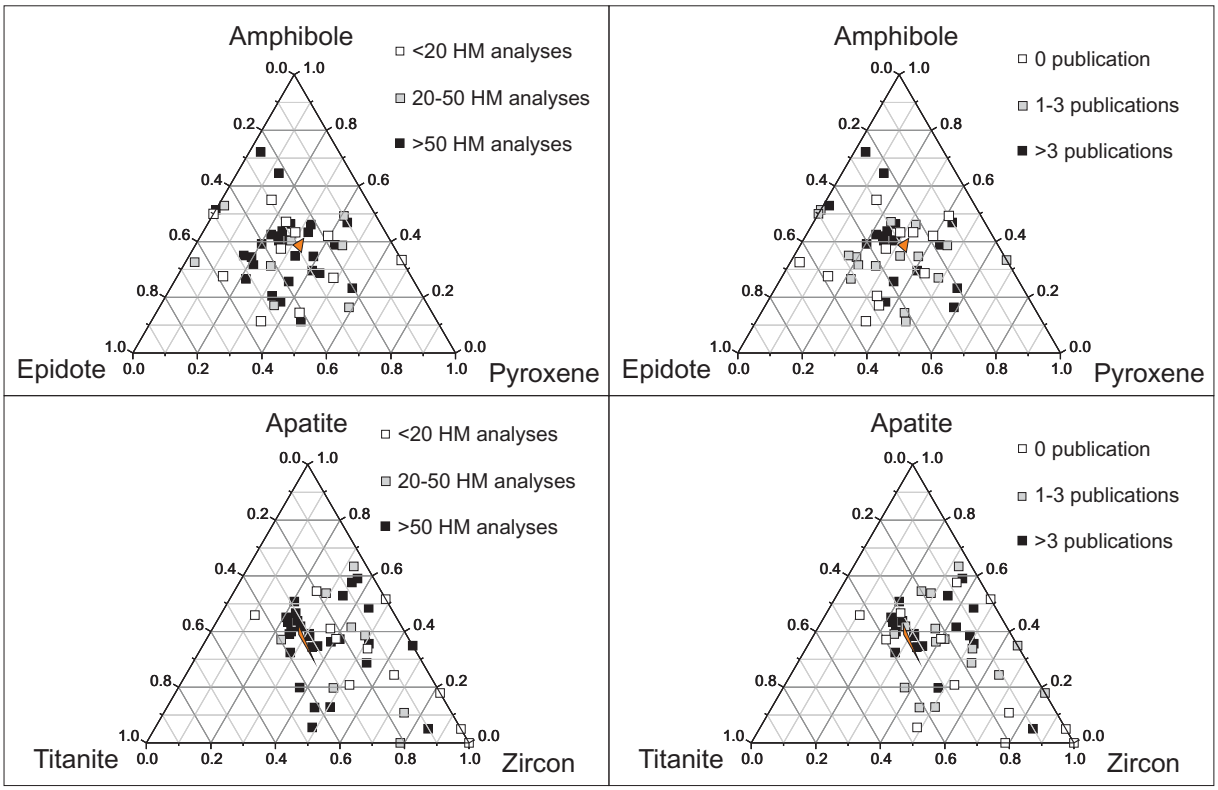

Fig. 12. The same ternary diagrams of HMR-2 major components as shown in Fig. 6, but restricted to the analyses determined by optical methods. The results are classified according to the experience of the contributors using two criteria: number of analyses performed so far (left) and number of published peer-reviewed papers with own HM data (right). The orange triangles represent the reference compositions between the wt%, nominal grain% and best-match average.

Table 7
Average absolute deviation of major component grain percentages from the nominal composition of the samples in [%] vs. method applied for sample splitting, data from optical methods only.

	Coning and quartering (10)	Micro riffler, splitter (25)	Other methods * (11)
HMR-1	3.0 ± 0.3	3.5 ± 0.4	3.7 ± 0.6
HMR-2	5.3 ± 0.7	5.6 ± 0.4	6.0 ± 0.8

Table 8
Average absolute deviation of major component grain percentages from the nominal composition of the samples in [%] vs. method applied for grain counting, data from optical methods only.

	Line (12)	Ribbon (21)	Fleet (11)
HMR-1	3.6 ± 0.7	3.4 ± 0.4	2.7 ± 0.4
HMR-2	6.2 ± 0.7	5.9 ± 0.5	4.7 ± 0.6

(7) The following suggestions should be considered for further improving techniques and applications in heavy mineral research:
- Most importantly for the optical analyses of heavy minerals, training of the operators is paramount. This can be done via university courses, individual training or specific short courses. Ideally, the laboratory routines should include some kind of (self-) evaluation, repeated regularly and using reference materials such as the HMR-samples. This holds for both beginners and experienced researchers.
- Before the full potential of automated high-throughput techniques in HM quantification can be achieved, a number of issues must be solved, mainly related to proper identification of the full range of heavy minerals.
- In view of the increasing demands for data documentation and numerous other methods that are becoming available for the analysis of single-grains, the documentation of grains and their position in the heavy mineral mounts by archiving photographs and/or coordinates should become a routine procedure in heavy mineral analysis.
- A follow-up interlaboratory test round within a few years should be undertaken to evaluate and hopefully demonstrate improvements in variability, comparability and precision of heavy mineral analyses.

Declaration of competing interest

The authors declare that they have no known competing financial interests or personal relationships that could have appeared to influence the work reported in this paper.

Acknowledgements

Some mineral samples were provided by the Mineral Collection of the Museum of the Geoscience Center, University of Göttingen, the Finnish Geological Survey and Gerhard Wörner. The careful preparation of the mineral samples has been performed by Judit Dunklné Nagy. The organizers are grateful for their kind help. Mette Olivarius and Robert Hall provided very careful and detailed reviews which greatly helped to clarify and improve the manuscript.

Appendix A. Appendices

A.1. Abbreviations and definitions

HM: heavy mineral.
%: grain percentage.
wt%: weight percentage.
N: number of all identified transparent or translucent heavy mineral grains in one analysis.
mineral sample: monomineralic grains produced by physical and chemical steps from one single rock piece or from one crystal.
component: representing one mineral species in the HMR samples; composed from one or more *mineral samples* (e.g. in the case of the amphibole *component* five different *mineral samples* were mixed).
major component: mineral species added to the *samples* with at least around 10 wt%.
minor component: mineral species added to the *samples* in minor amounts (between ca. 1 and 4 wt%).
sample: HMR-1 and HMR-2 synthetic mixture made from the *components* and distributed for the *contributors* for the purpose of the interlaboratory round robin test.
contributor: operator or group of operators, who performed the heavy mineral analysis, reported the results and agreed to their presentation; their identity will be kept confidential.
nominal value: approximate grain percentages of the *components* in the HMR *samples*, which were calculated from the weight percentages.
best-match average: calculated as arithmetic mean from the analyses that match the following criteria: all *major components* and more than five *minor components* were identified and less than 5% non-added minerals were counted.

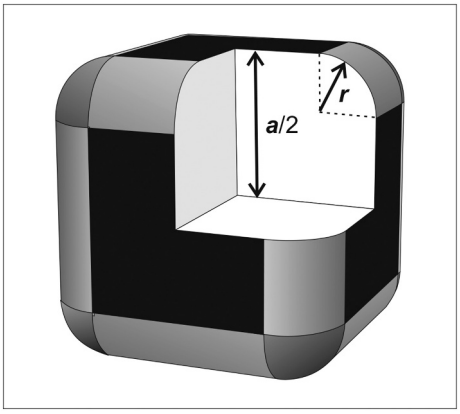

Fig. A.1. Fig. A.1 Schematic presentation of a spherocube (drawing simplified after Marechal et al., 2012). The black squares represent the rest of surface from the truncated cube. The ratio of ***a*** and ***r*** expresses the transformation from cube to sphere.

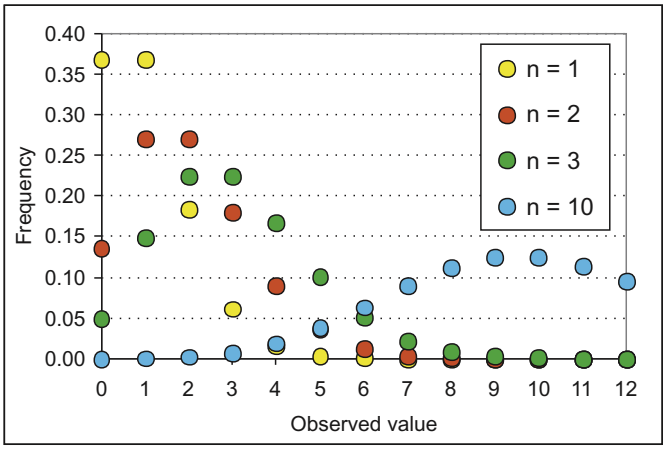

Fig. A.2. Fig. A.2 Some examples for the calculated frequencies of Poisson distribution when the number of expected grains (n) is low.

Appendix B. Calculation of the nominal grain percentages

The densities of several, quasi-stoichiometric minerals species are actually invariable (e.g. rutile, kyanite, corundum, fluorite). In the case of minerals having variable chemical composition (dominantly controlled by Mg/Fe substitution, like olivine or pyroxene) we have considered the optical properties and in some cases EMP analyses to estimate the densities. In the case of zircon, the density is mostly controlled by the density of radioactive damages (e.g. Murakami et al., 1991). The euhedral component (sample Zrn-eu) is derived from Cretaceous, shallow granitoid bodies from the Lhasa batholith (Tibet). Due to the relatively low average damage density these zircons have approx 4.5 g/cm^3 density. The other zircon component of rounded grains (DM-126) was derived from an Australian beach placer and represent provenance from a cratonic catchment with old cooling ages. Since these zircons have less ordered crystal structure, we assigned a density of 4.2 g/cm^3 to this mineral sample.

For the calculation of the average grain volumes of the components we took microphotographs on randomly selected grains embedded in Meltmount thermoplastic resin (n = 1.66). From each component the size and morphology of 60 grains were observed by the ImageJ software (Schindelin et al., 2012). The area, major- and minor axes, circularity, aspect ratio, roundness and solidity were recorded. These information are actually a 2D representation of the projected shape of the grains, resting typically on their flat side. The maximum thickness of the grains (in Z direction) was determined in air on randomly selected grains scattered on slides by the Zeiss ZEN software using a Zeiss Axio Imager M2m microscope with *Z*-stepper integrated in the microscope body.

In order to express the volume of the grains from the 2D parameters determined by the microphotographs and the Z values, we assumed that the transformation of an object determined by tips, edges and facets to an ellipsoid having only a completely convex surface can be described by a spherocube (Marechal et al., 2012). The aspect ratio of the non-equal axes has no impact on the calculation, it can be modelled actually by a cube to sphere transformation. Thus the 2D → 3D approach is based on the equation:

$$y = 2.218 * x - 1.215$$

where

y = multiplication factor for volume calculation.
x = projected_area/(long axis*short axis) [on the microscopic image].
the constants of the equation are determined by linear regression assuming spherocubes with different a/r ratios (see Appendix Fig. A.1).
The volume of the grain then is calculated as:

$$V = y * a * b * c$$

where

a, b and c are the axes representing the maximum extension of the grain [μm].
The number of the grains of a given mineral sample is calculated as:

$$n = m * p * 1{,}000{,}000/(V * d)$$

where

n = number of grains in a mineral sample.
m = mass of mineral sample [g].
p = proportion of the mineral species in the mineral sample (0–1).
V = calculated volume of one average grain of the mineral sample [10^6 μm^3].
d = density [g/cm^3].
The grain percentage of a mineral sample in the nominal concentration is calculated as:

$$grain\% = 100 * n_i/\Sigma n_i$$

where

n_i = calculated number of grains in the i-th mineral sample.
Σn_i = calculated number of all grains in a HMR sample.

Appendix C. Calculation of the confidence interval of the grain percentages

We applied two methods to calculate the 95% confidence intervals for the grain percentages. For analyses having less than 1500 counted transparent and translucent heavy mineral grains the Excel CHIINV function yield proper calculations.
lower and upper confidence intervals are:

$$LCI_i = X_i * CHIINV(1 - (alpha/2), 2 * (n_i + 1))/2/n_i$$

$$UCI_i = X_i * CHIINV(alpha/2, 2 * (n_i + 1))/2/n_i$$

where

LCI_i and UCI_i are the confidence intervals of the i-th mineral species.
X_i = percentage of the i-th mineral species.
n_i = number of counted grains of the i-th mineral species.
alpha = confidence level (0.05).
However, when the numbers of total grain counts were higher this function is not able to calculate the result and we have to use a simpler approximation. Remarkably this method has negligible deviation from the calculation procedure indicated above.

$$LCI_i = n_i + 1–1.96 * SQRT(n_i + 1) * (100/N)$$

$$UCI_i = n_i + 1 + 1.96 * SQRT(n_i + 1) * (100/N)$$

where

N = number of all counted transparent and translucent heavy mineral grains.
constant 1.96 is from Selby (1972).

Supplementary data

Supplementary data to this article can be found online at https://doi.org/10.1016/j.earscirev.2020.103210.

References

Allen, P.A., 2017. Sediment Routing Systems. Cambridge University Press, Cambridge 407pp.

Andò, S., 2020. Gravimetric separation of heavy minerals in sediments and rocks. Minerals 10, 273. https://doi.org/10.3390/min10030273.

Andò, S., Garzanti, E., 2014. Raman spectroscopy in heavy mineral studies. Geol. Soc. Lond., Spec. Publ. 386, 395–412.

Andò, S., Bersani, B., Vignola, P., Garzanti, E., 2009. Raman spectroscopy as an effective tool for high-resolution heavy-mineral analysis: examples from major Himalayan and Alpine fluvio-deltaic systems. Spectrochim. Acta A Mol. Biomol. Spectrosc. 73, 450–455.

Andò, S., Vignola, P., Garzanti, E., 2011. Raman counting: a new method to determine provenance of silt. Rend. Lincei 22, 327–347.

Andò, S., Garzanti, E., Padoan, M., Limonta, M., 2012. Corrosion of heavy minerals during weathering and diagenesis: a catalogue for optical analysis. Sediment. Geol. 280, 165–178.

Artini, E., 1891. Intorno alla composizione mineralogica delle sabbie del Ticino. In: Giornale di Mineralogia, Cristallografia e Petrologia Pavia, II, pp. 177–195.

ASTM E1301-95, 2003. Standard Guide for Proficiency Testing by Interlaboratory Comparison. ASTM International, West Conshohocken, PA, USA.

ASTM Standard D7778, 2012. Standard Guide for Conducting an Interlaboratory Study to Determine the Precision of a Test Method. ASTM International, West Conshohocken, PA, USA.

ASTM Standard E691, 2013. Standard Practice for Conducting an Interlaboratory Study to Determine the Precision of a Test Method. ASTM International, West Conshohocken, PA, USA.

Bernstein, S., Frei, D., McLimans, R.K., Knudsen, C., Vasudev, V.N., 2008. Application of CCSEM to heavy mineral deposits: source of high-Ti ilmenite sand deposits of South Kerala beaches, SW India. J. Geochem. Explor. 96, 25–42.

Boenigk, W., 1983. Schwer Mineral Analyse. Ferdinand Enke Publishers, Stuttgart 158 pp.

Boswell, P.G.H., 1933. On the Mineralogy of Sedimentary Rocks. Murby and Co., London 393 pp.

Caracciolo, L., Andò, S., Vermeesch, P., Garzanti, E., Mc Cabe, R., Barbarano, M., Paleari, C., Rittner, M., Pearce, T., 2019. A multidisciplinary approach for the quantitative provenance analysis of siltstone: Mesozoic Mandawa Basin, southeastern Tanzania. In: Dowey, P., Osborne, M., Volk, H. (Eds.), Application of Analytical Techniques to Petroleum Systems. Geological Society, London, Special Publications, 484https://doi.org/10.1144/SP484-2018-136.

Chayes, F., 1949. A simple point counter for thin-section analysis. Am. Mineral. 34, 1–11.

De Filippi, F., 1839. Sulla costituzione geologica della pianura e delle colline della Lombardia. Ann. Univ. Stat. 59, 225–248.

Dick, A.B., 1887. On zircon and other minerals contained in sand. Nature 36, 91–92.

Dickinson, W.R., Suczek, C.A., 1979. Plate tectonics and sandstone composition. AAPG Bull. 63, 2164–2182.

Dodson, M.H., Compston, W., Williams, I.S., Wilson, J.F., 1988. A search for ancient detrital zircons in Zimbabwean sediments. J. Geol. Soc. Lond. 145, 977–983.

Finkelman, R.B., Fiene, F.L., Miller, R.N., Simon, F.O., 1984. Interlaboratory comparison of mineral constituents in a sample from the Herrin (No. 6) coal bed from Illinois. In: USGS Circular 932, 42 pp.

Fleet, W.F., 1926. Petrological notes on the Old Red Sandstone of the West Midlands. Geol. Mag. 63, 505–516.

Galbraith, R.F., 1988. Graphical display of estimates having differing standard errors. Technometrics 30, 271–281.

Galbraith, R.F., 1990. The radial plot: graphical assessment of spread in ages. Nucl. Tracks Radiat. Meas. 17, 207–221.

Garzanti, E., Andò, S., 2019. Heavy minerals for junior woodchucks. Minerals 9, 148.

Garzanti, E., Andò, S., Vezzoli, G., 2008. Settling-equivalence of detrital minerals and grain-size dependence of sediment composition. Earth Planet. Sci. Lett. 273, 138–151.

Garzanti, E., Andò, S., Vezzoli, G., 2009. Grain-size dependence of sediment composition and environmental bias in provenance studies. Earth Planet. Sci. Lett. 277, 422–432.

Gonfiantini, R., et al., 2003. Intercomparison of boron isotope and concentration measurements. Part II: Evaluation of results. Geostand. Newslett. 27, 41–57. https://doi.org/10.1111/j.1751-908X.2003.tb00711.x.

Hackley, P.C., Araujo, C.V., Borrego, A.G., Bouzinos, A., Cardott, B.J., Cook, A.C., Eble, C., et al., 2015. Standardization of reflectance measurements in dispersed organic matter: results of an exercise to improve interlaboratory agreement. Mar. Pet. Geol. 59, 22–34. https://doi.org/10.1016/j.marpetgeo.2014.07.015.

Heroy, D.C., Kuehl, S.A., Goodbred Jr., S.L., 2003. Mineralogy of the Ganges and Brahmaputra Rivers: implications for river switching and Late Quaternary climate change. Sediment. Geol. 155, 343–359.

Hubert, J.F., 1962. A zircon-tourmaline-rutile maturity index and the interdependence of the composition of heavy mineral assemblages with the gross composition and texture of sandstones. J. Sediment. Res. 32, 440–450.

ISO 13528, 2015. Statistical Methods for Use in Proficiency Testing by Interlaboratory Comparison. International Organization for Standardization, Geneva, pp. 1–89.

ISO 21748, 2017. Guidance for the Use of Repeatability, Reproducibility and Trueness Estimates in Measurement Uncertainty Evaluation. International Organization for Standardization, Geneva, pp. 1–38.

ISO/IEC 17043, 2010. Conformity Assessment-General Requirements for Proficiency Testing, First edition. ISO Committee on conformity assessment (CASCO), Geneva, pp. 1–39.

ISO/TR 22971, 2005. Accuracy (Trueness and Precision) of Measurement Methods And results—Practical Guidance for the Use of ISO 5725-2:1994 in Designing, Implementing, and Statistically Analyzing Interlaboratory Repeatability and Reproducibility Results. International Organization for Standardization, Geneva, Switzerland.

Ketcham, R.A., Carter, A., Hurford, A.J., 2015. Inter-laboratory comparison of fission track confined length and etch figure measurements in apatite. Am. Mineral. 100, 1452–1468.

Košler, J., Sláma, J., Belousova, E., Corfu, F., Gehrels, G.E., Gerdes, A., Horstwood, M.S.A., Sircombe, K.N., Sylvester, P.J., Tiepolo, M., Whitehouse, M.J., Woodhead, J.D., 2013. U-Pb detrital zircon analysis – results of an inter-laboratory comparison. Geostand. Geoanal. Res. 37, 243–259.

Krogh, T.E., 1982. Improved accuracy of U–Pb zircon ages by the creation of more concordant systems using an air abrasion technique. Geochim. Cosmochim. Acta 46, 637–649.

Ludwig, K.R., 2012. User's manual for Isoplot 3.75: a geochronological Toolkit for Microsoft Excel. In: Berkeley Geochronology Center Special Publication, no. 4, (70pp).

Lünsdorf, N.K., Kalies, J., Ahlers, P., Dunkl, I., von Eynatten, H., 2019. Semi-automated heavy-mineral analysis by Raman spectroscopy. Minerals 9, 385.

Mange, M.A., Maurer, H.F.W., 1992. Heavy Minerals in Colour. Chapman and Hall, London 147pp.

Mange, M.A., Wright, D.T., 2007. Heavy minerals in use. In: Developments in Sedimentology. Vol. 58 Elsevier, Amsterdam 1283 pp.

Mange-Rajetzky, M.A., 1981. Detrital blue sodic amphibole in recent sediments, southern coast, Turkey. J. Geol. Soc. 138, 83–92.

Marechal, M., Zimmermann, U., Löwen, H., 2012. Freezing of parallel hard cubes with rounded edges. J. Chem. Phys. 136, 144506. https://doi.org/10.1063/1.3699086.

McIntyre, G.A., Brooks, C., Compston, W., Turek, A., 1966. The statistical assessment of Rb-Sr isochrons. J. Geophys. Res. 71, 5459–5468.

Meunier, S., 1877. Composition et Origine du Sable Diamantifère de Du Toit's Pan (Afrique Australe). C. R. Acad. Sci. 84 (6), 250–252.

Miller, D.S., Eby, N., McCorkell, R.H., Rosenberg, P.E., Suzuki, M., 1990. Results of interlaboratory comparison of fission track ages for the 1988 fission track workshop on a putative apatite standard for internal calibration. Nucl. Tracks Radiat. Meas. 17, 237–245.

Milner, H.B., 1929. Sedimentary Petrography. Murby and Co., London 514 pp.

Morton, A.C., 1985. A new approach to provenance studies: electron microprobe analysis of detrital garnets from Middle Jurassic sandstones of Northern Sea. Sedimentology 32, 553–566.

Morton, A.C., 2012. Value of heavy minerals in sediments and sedimentary rocks for provenance, transport history and stratigraphic correlation. In: Sylvester, P. (Ed.), Quantitative Mineralogy and Microanalysis of Sediments and Sedimentary Rocks. Mineralogical Association of Canada Short Course Series, 42pp. 133–165.

Morton, A.C., Hallsworth, C.R., 1994. Identifying provenance-specific features of detrital heavy mineral assemblages in sandstones. Sediment. Geol. 90, 241–256.

Mounteney, I., Burton, A.K., Farrant, A.R., Watts, M.J., Kemp, S.J., Cook, J.M., 2018. Heavy mineral analysis by ICP-AES a tool to aid sediment provenancing. J. Geochem. Explor. 184, 1–10.

Murakami, T., Chakoumakos, B.C., Ewing, R.C., Lumpkin, G.R., Weber, W.J., 1991. Alpha-decay event damage in zircon. Am. Mineral. 76, 1510–1532.

Paleari, C.I., Delmonte, B., Andò, S., Garzanti, E., Petit, J.R., Maggi, V., 2019. Aeolian dust provenance in central east Antarctica during the Holocene: environmental constraints from single-grain Raman spectroscopy. Geophys. Res. Lett. 46, 9968–9979.

Retgers, J.W., 1895. Ueber die mineralogische und chemische Zusammensetzung der Dünensande Hollands und über die Wichtigkeit von Fluss- und Meeressand-Untersuchungen im Allgemeinen. N. Jb. Mineral. Geol. Palaeontol. 1895 (1), 16–74.

Rubey, W.W., 1933. The size-distribution of heavy minerals within a water-laid sandstone. J. Sediment. Petrol. 3, 3–29.

Schindelin, J., Arganda-Carreras, I., Frise, E., et al., 2012. Fiji: an open-source platform for biological-image analysis. Nat. Methods 9, 676–682. PMID 22743772. https://doi.org/10.1038/nmeth.2019.

Selby, S.M., 1972. Standard Mathematical Tables. 728 pp. The Chemical Rubber Co., Cleveland, Ohio.

Sylvester, P., 2012. Use of the mineral liberation analyzer (MLA) for mineralogical studies of sediments and sedimentary rocks. In: Sylvester, P. (Ed.), Quantitative Mineralogy and Microanalysis of Sediments and Sedimentary Rocks. Mineralogical Association of Canada Short Course Series, 42pp. 1–16.

Szewczak, E., Bondarzewski, A., 2016. Is the assessment of interlaboratory comparison results for a small number of tests and limited number of participants reliable and rational? Accred. Qual. Assur. 21, 91–100.

Thürach, H., 1884. Über das Vorkommen mikroskopischer Zirkone und Titanmineralien in den Gesteinen. Verh. Phys. Med. Ges. Würzburg 18, 203–284.

Tolosana-Delgado, R., 2012. Uses and misuses of compositional data in sedimentology. Sediment. Geol. 280, 60–79.

Vail, P.R., Mitchum, R.M., Thompson, S., 1977. Seismic stratigraphy and global changes of sea level, Part 3: relative changes of sea level from coastal onlap. In: Payton, C.E. (Ed.), Seismic Stratigraphy - Applications to Hydrocarbon Exploration. American Association of Petroleum Geologists, Memoir, 26pp. 63–81.

Vermeesch, P., 2009. Radial Plotter: a Java application for fission track, luminescence and other radial plots. Radiat. Meas. 44, 409–410.
Vermeesch, P., 2018. Statistical models for point-counting data. Earth Planet. Sci. Lett. 501, 112–118.
Vermeesch, P., Rittner, M., Petrou, E., Omma, J., Mattinson, C., Garzanti, E., 2017. High throughput petrochronology and sedimentary provenance analysis by automated phase mapping and LAICPMS. Geochem. Geophys. Geosyst. 18, 4096–4109.
von Eynatten, H., Dunkl, I., 2012. Assessing the sediment factory: the role of single grain analysis. Earth-Sci. Rev. 115, 97–120.
Walker, R.G. (Ed.), 1979. Facies Models. Geoscience Canada, Reprint Series, 1, (211pp).
Webster, J.R., Knight, R.P., Winburn, R.S., Cool, C.A., 2003. Heavy mineral analysis of sandstones by Rietveld analysis. Adv. X-ray Anal. 46, 198–203.
Wendt, I., Carl, C., 1991. The statistical distribution of the mean squared weighted deviation. Chem. Geol. 86, 275–285 (Isotope Geoscience Section).
Zhang, X.J., Pease, V., Omma, J., Benedictus, A., 2015. Provenance of Late Carboniferous to Jurassic sandstones for southern Taimyr, Arctic Russia: a comparison of heavy mineral analysis by optical and QEMSCAN methods. Sediment. Geol. 329, 166–176.